Final Report

ECM3102

Title: CFD Analysis of CX501 Generator Set Package Ventilation for Centrax Gas Turbines

Date of submission: 02/05/2013

Student Name: Heather Bolt
Programme: MEng Mechanical Engineering
Student number: 610033357
Candidate number: 009281

Supervisor: Dr. Gavin Tabor

Abstract

This project is for Centrax Gas Turbines, an engineering company based in Newton Abbot. The aim of this project was to comment on the feasibility of adding boost compressor bleed air into the ventilation air of the CX501 gas turbine power generation package. To accomplish this, the package ventilation was analysed using Computational Fluid Dynamics (CFD). Two CFD models of the package ventilation, with and without boost compressor air bleed, were created and compared. This comparison enabled several comments to be made on the effect of adding boost compressor air bleed into the package ventilation. Firstly the outlet temperature of the ventilation air for the model with boost compressor air bleed, was 15K higher than the model without boost compressor air bleed. Secondly adding boost compressor bleed air to the package ventilation increased the average velocity on the surface of the tread plate from 4.4 m/s to 9.7 m/s. Thirdly bleeding air from the boost compressor into the package ventilation caused greater mixing of the ventilation air within the package, which prevented hot pockets of air forming in areas of low air velocity around the gas turbine engine. When compared with experimental results, the temperature of the ventilation air at the outlet of the model was found to be 3.6K less in the CFD models. It was deemed that this discrepancy between the CFD model and the actual package ventilation, was due to inconsistencies between the surface of the gas turbine engine in the CFD models and the actual surface of the gas turbine engine.

Keywords:

CFD, Ventilation, FLUENT, Gas Turbines

Acknowledgements

Special thanks must be given to Dr. Gavin Tabor whose help with CFD in this project has been invaluable.

Table of contents

List of Figures

1 Introduction

This project is for Centrax Gas Turbines, an engineering company based in Newton Abbot, who manufacture ‘gas turbine power generation packages ranging from 3.9 MW to 64.0 MW for both the Industrial and Oil & Gas Energy markets’ [1]. Centrax want to bleed air from the boost compressor attached to the gas turbine engine, into the package ventilation for the CX501 gas turbine power generation package. However the effect this will have on the cooling and airflow of the package ventilation is unknown. The aim of this project is to comment on the feasibility of adding boost compressor bleed air into the package ventilation for the CX501 package. Figure 1.1 below is a labeled diagram of the CX501 package.

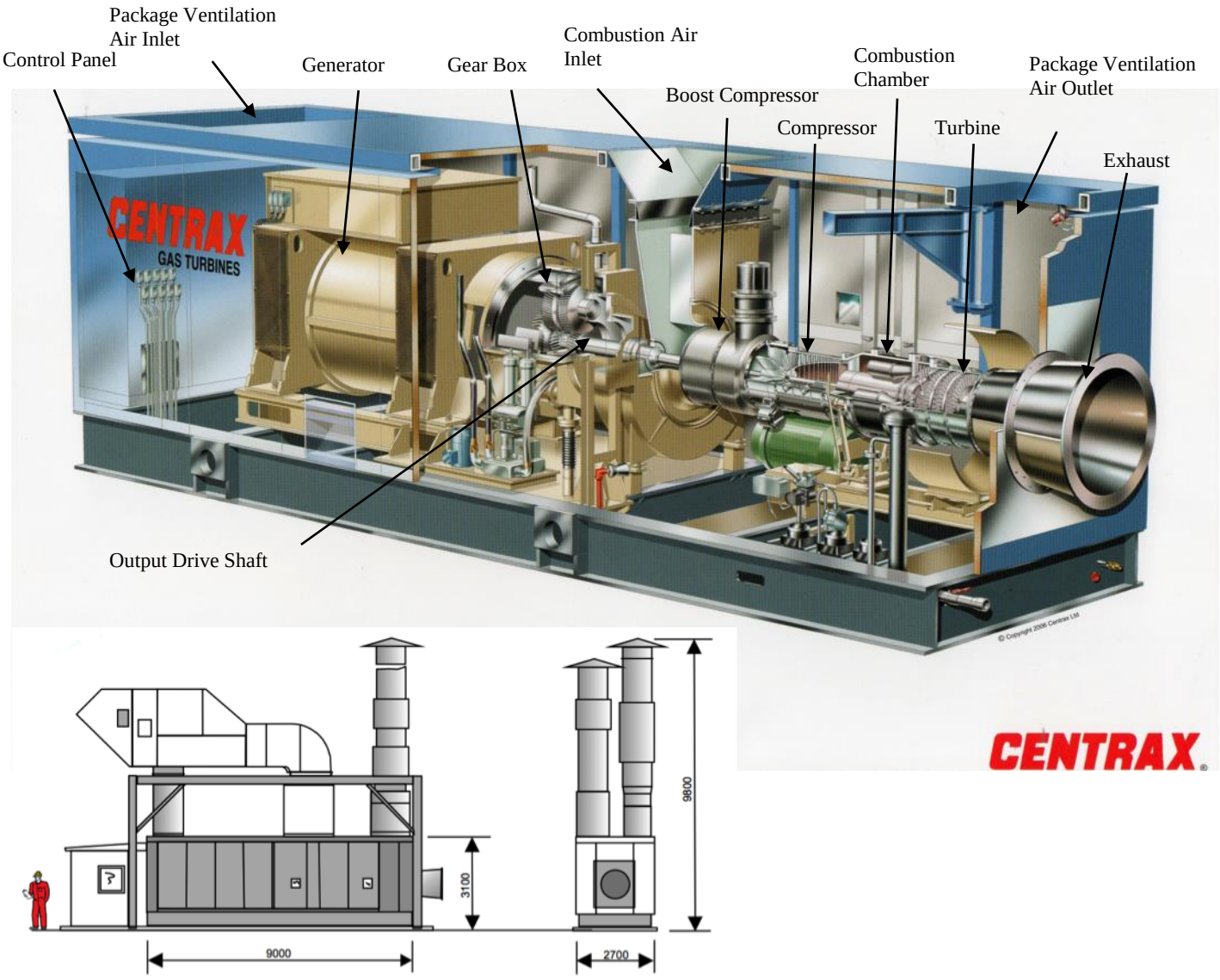

Figure 1.1 – Labeled diagram of a CX501 Generator Set

The CX501 uses a Rolls-Royce 501 KB7S [2] gas turbine engine with a boost compressor. Part load (less than full power) is required for performance and emissions control - in order to operate the gas turbine engine at part load air is bled from the 14th stage of the compressor. Air that is bled from the 14th stage of the compressor is fed directly into the combustion air intake (a blue line in Figure 1.2 represents this process). Using this method Centrax can only achieve a maximum of 30% turndown[1], however they want to achieve a turndown of 50%. In order to achieve the required 50% turndown Centrax need to be able to achieve 20% turndown by bleeding air from elsewhere. The other bleed air option is a valve on the boost compressor, this air would bleed straight into the package ventilation (this process is represented by a red line in Figure 1.2).

Bleeding air into the package ventilation may have an adverse effect on the cooling and ventilation airflow. The package ventilation removes heat rejected form the gas turbine engine and also provides sufficient airflow to disperse any minor gas leaks: such as from pipes, fittings or flanges. A fan at the outlet, operating on a fixed volumetric flow rate, draws air through the package. Consequently, bleeding air from the boost compressor will reduce the mass flow rate of the air through the package. The boost compressor air bleed will also be at a higher temperature than the package ventilation air and will therefore increase the temperature of the air inside the package.

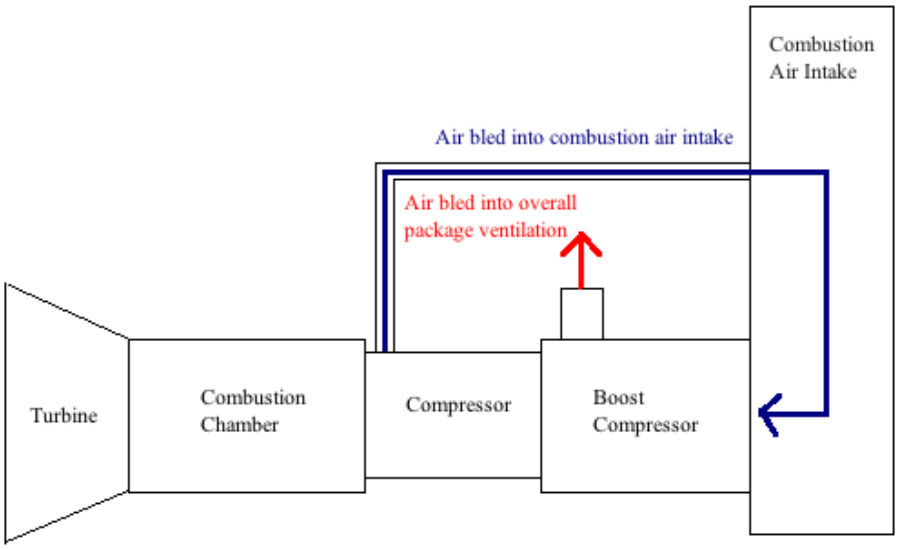

Figure 1.2 – Schematic of the gas turbine used in the CX501 package with different bleed air options

The main objective of this project is to create two CFD models and compare these models to assess the effect of adding boost compressor air bleed on the package ventilation. Centrax specified in the initial project meeting [3] that they are only concerned with the package ventilation through the hazardous area of the package; this is the area from the combustion air inlet to the exhaust (containing the gas turbine). Therefore, only the hazardous area of the

[1] 'Turndown' is a term for bleeding air from the gas turbine engine; 30% turndown corresponds to a power output of 70%.

package will be modeled. The two models, with and without boost compressor air bleed, will be compared to assess the effect of bleeding air from the boost compressor into the package ventilation.

Following this introduction there is a brief overview which will introduce some basic concepts of CFD. A literature review will then critically analyse what has been done by other researches using CFD to model ventilation through gas turbine packages and other spaces. Thirdly, there is a section on the methodology used in this project. The design section will highlight the processes involved in creating the CFD models and demonstrate the application of knowledge that has been gained through the duration of this project. The final models are then presented in the results section and analysed to assess the effect of adding boost compressor air bleed into the package ventilation. Finally, sustainability is discussed and project conclusions are drawn.

2 Background

2.1 Overview of Computational Fluid Dynamics (CFD)

The CFD software used in this project was ANSYS FLUENT [4] which uses the finite volume method, as do most commercially available CFD codes. The finite volume method involves dividing the fluid domain into a finite number of control volumes (called elements) connected by nodes; this process is called meshing. Figure 2.1 below shows a vortex flow separator meshed using a coarse mesh and a fine mesh. Fluid flow is described by the Navier-Stokes equations, which are 2nd order partial differential equations that govern fluid flow. These governing fluid equations are integrated over each element to create a set of ordinary differential equations (ODE) for the unknown variables in each element (such as velocity, pressure and temperature). The ODEs are discretised to produce a system of nonlinear algebraic equations, which are then linearised and solved iteratively. When running a calculation, a graph of residuals against iteration number is plotted on the screen. The basic principles of CFD and the finite volume method can be found in several textbooks, such as *An introduction to computational fluid dynamics: the finite volume method* by H.K. Versteeg, and W. Malalalsekera [5].

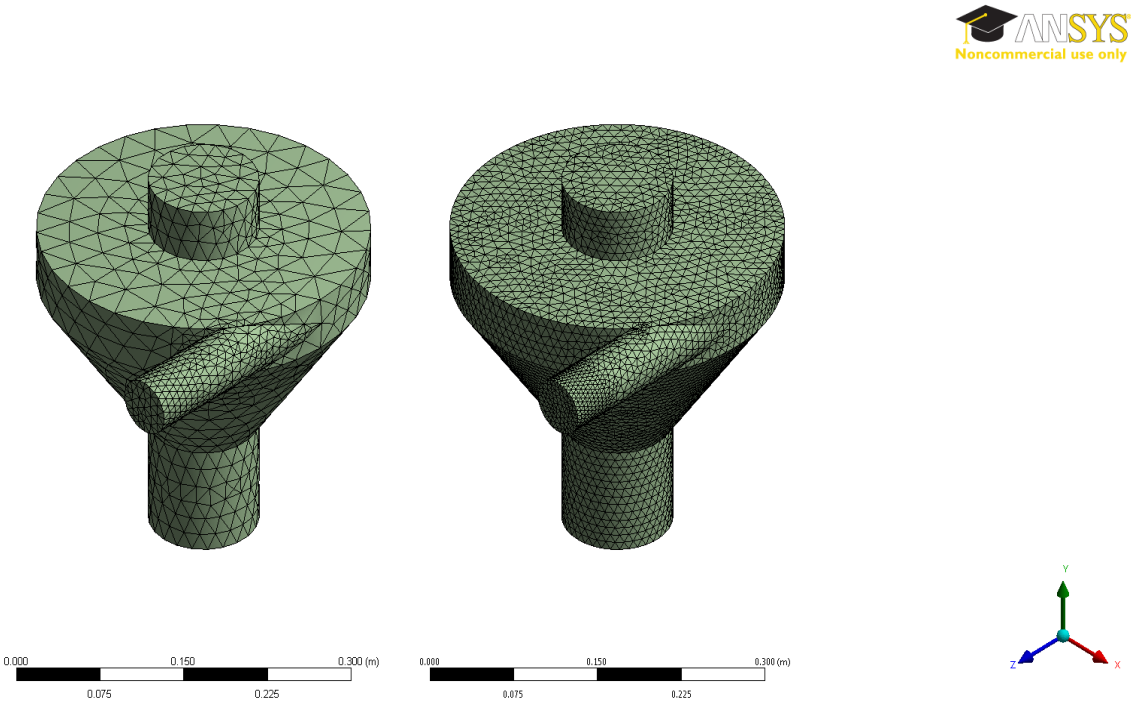

Figure 2.1- Vortex flow separator meshed with a coarse mesh (image on the left) and a fine mesh (image on the right)

2.2 Literature Review

2.2.1 CFD

Computational Fluid Dynamics is a powerful tool used to model fluid flow and today it is widely used in a variety of applications. CFD is 'the analysis of systems involving fluid flow heat transfer and associated phenomena such as chemical reactions by means of computer based simulation' [6]. CFD has been widely used in the heating and ventilation control sector as it has proved to be a feasible and useful method for investigating ventilation performance [7]. In contrast to full scale testing, CFD is a much more cost-effective method for investigating ventilation flows. One major drawback of CFD is that the user is limited by the power of their computer, indeed as one study by Sun *et al.* [7] found 'CFD simulation of ventilated space is still too slow in computing on today's personal computers.'

2.2.2 Turbulence Models

Fluid flow can be classified into three states; laminar, transitional and turbulent. Whereas laminar flow is characterised by the orderly motion of particles in fluid flow, turbulent flow is characterised by the random, chaotic movement of particles in fluid flow. Modeling turbulent flow is therefore much more complex than modeling laminar flow, consequently there are numerous turbulence models available in CFD. The lack of a single turbulence model is because 'the necessary computer storage exceeds by many orders of magnitude what is available' [8]. The choice of turbulence model depends on several factors, such as: the time available for calculations, the computational power of the computer and the physical properties of the fluid. The standard turbulence model is the k-ε model, which is a two-equation model, solving a transport equation for k (turbulent kinetic energy) and ε (turbulent dissipation). When modeling flow in gas turbine enclosures 'the k-ε model is recommended as a minimum standard . . . more advanced turbulence models can be used if they are known to be appropriate' [9].

One variation of the standard k-ε model is the RNG (Re-Normalisation Group) k-ε model. This model accounts for smaller scale turbulence, which is not included in the standard model. A study by Behnia *et al.* [10] into CFD simulations of heat transfer from a heated module in an air stream, compared the standard and RNG k-ε model and found no significant difference between the models. Whereas a study by Li *et al.*[11] into the thermal environment in an air conditioned train station building, found that the RNG (Re-Normalisation Group) k-ε model gave the most accurate results when compared with experimental results.

The k-ω model is also a two-equation model; solving a transport equation for k (turbulent kinetic energy) and ω (specific dissipation). The SST (Shear Stress Transport) k-ω model is a combination of the standard k-ω model, which is used near walls, and the k-ε model, which is used in the free stream. A study by Stamou *et al.* [12] into indoor airflow and heat transfer, found that the SST k-ω model showed the best agreement with experimental results. There are several advantages to the k-ω model. For example, 'it tends to produce converged solutions more rapidly than the k-ε model' [12] and it does not need the addition of wall functions. In

other words, it is valid for flows in the viscous sublayer of boundary layer flow unlike the k-ε models.

A study by Defraeye *et al.* [13] into the convective heat transfer at the surface of a cube immersed in a turbulent boundary layer, investigated the standard k-ε model, the RNG k-ε model and the SST k-ω model. This study found that the SST k-ω model gave the most accurate results for the surface temperature of the cube, however it was the standard k-ε model that gave the best agreement with overall experimental results.

2.2.3 Meshing

The accuracy of the solution calculated using CFD depends on the number of elements in the mesh; the greater the number of elements the more accurate the solution. However, as the number of elements in the mesh increases so does the time it takes to compute the results. Therefore the number of elements in a mesh is always a compromise between computational resources and accuracy. The total number of elements required for a successful compromise depends on the shape and size of the domain. CFD guidelines for gas turbine package ventilation models state that the minimum number of elements for a CFD simulation is ¼ million with ½ to 3 million elements being the norm [9]. CFD gas turbine package ventilation studies corroborate this information; one study had around ¼ million elements [14] and another around 370,000 [15]. It is not only the quantity of elements that affect the accuracy of the final solution but also the quality. The quality of a mesh depends on various criteria such as 'the shape of the cells (aspect ratio, skewness, warp angle or included angle of adjacent faces), distances of cell faces from boundaries, and spatial distribution of cell sizes' [16].

2.2.4 Heat Transfer

2.2.4.1 Near Wall Meshing

Careful consideration of the thermal boundary layer that develops on the surface of a heated object is important when modeling heat transfer. Particles at the surface of a heated object will share the same temperature as the surface, while at some distance away from the surface the fluid particles will have the same temperature as the free stream flow. The particles at the surface will transfer energy to adjacent fluid particles, thereby creating a temperature gradient. The region in which this temperature gradient exists is called the thermal boundary layer. Heat that is conducted from the hot surface to the thermal boundary layer is carried downstream and transferred to fluid outside of the boundary layer. Thus 'appreciation of boundary layer phenomena is essential to understanding convection heat transfer' [17]. It is therefore important to examine the mesh around any heated object in order to successfully compute heat transfer from that object. In FLUENT there are several ways to model near-wall flow. One option is to use a low-Reynolds number model, however this 'imposes a severe restriction on the near-wall grid spacing by requiring several grid points in the viscous sublayer' [10]. In other words, this method requires a very fine mesh adjacent to the wall, and in cases with complex geometries it is not practical for general use [9] [13].

Where a low-Reynolds number model is not suitable, wall functions are used. These wall functions bridge the flow results between the flow properties on the wall, and the flow properties in near wall elements. Standard wall functions are the most widely used in industrial flows [18].

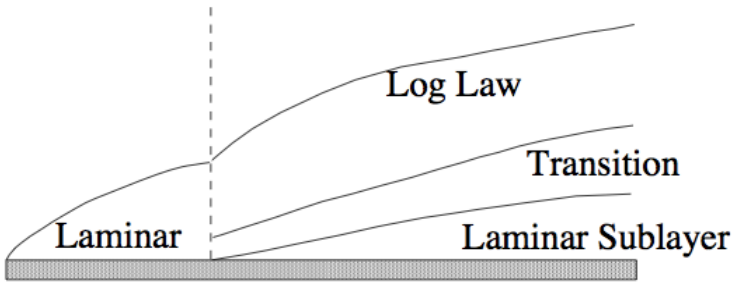

Figure 2.2 – Boundary layer flow [20]

For standard wall functions it is important that the centre point of the element next to the wall is inside the log law region of the boundary layer (see Figure 2.2). This condition is evaluated by the y^+ value, which is the non-dimensional distance from the wall to the first node in the mesh. The acceptable values of y^+ for standard wall functions are open to interpretation; Li *et al* [11] define acceptable y^+ values as being between 30 and 150, another source gives $20 < y^+ < 200$ [9]. On the other hand a study by Drefraeye *et al.* recommends that the y* values are used for the evaluation of the near wall mesh instead of the y^+ value, stating that 'as the y* value is used by the wall functions . . . the wall-adjacent cell should have a [y*] value of about 30-500' [13]. Scalable wall functions and enhanced wall functions can also be used which are still reliable even if the centre point of the element next to the wall is within the viscous sublayer. It is interesting to note that the SST k-ω turbulence model uses enhanced wall treatment as default [19] and therefore can account for low-Reynolds number effects.

2.2.4.2 Buoyancy

Buoyancy is another important feature to be considered when modeling heat transfer. Best practice guidelines for CFD concerning the analysis of ventilation in gas turbine enclosures state that 'the effects of buoyancy should always be incorporated in a CFD model for GT enclosures' [9]. A study by Vahidi *et al.* [14] into the ventilation of a turbine package enclosure found that although natural convection had little effect on the overall flow behaviour, it played an important part in the air temperature distribution. There are various ways to model buoyancy effects in CFD; for example a study by Mishra *et al.* [21] into the cooling of internal combustion engines included gravity (at 9.8 m/s^2) to consider buoyancy effects.

2.2.4.3 Radiative Heat Transfer

Any object above absolute zero will emit thermal radiation. In a gas turbine package enclosure, the thermal radiation emitted from the gas turbine engine will increase the temperature of the enclosure walls and surrounding objects. Typically however, a radiation model is not used as 'if the surface heat fluxes or temperatures can be specified . . . there will be no need for a radiation model' [9]. It is not usual practice to include a radiation model when using CFD to model the package ventilation through gas turbine enclosures, unless specific surface temperatures around the package are required.

2.2.5 Convergence

It is necessary to use some measure to gauge whether a satisfactory solution has been reached. Generally this process involves monitoring the residuals for the equations being solved (such as continuity, velocity, energy and turbulence). Figure 2.3 below is an example of the graph of residuals provided by FLUENT for a steady state solution that has successfully converged. These residuals 'indicate how far the present approximate solution is away from exact cancellation of flux balances in each cell' [16]. The solution is deemed to have converged when the average value of the residuals falls below a certain value, but there are no set rules for what this value is. A study by Vahidi *et al.* [14] into ventilation of a gas turbine package enclosure deemed the solution to have converged when all residuals were below 10^{-3}. On the other hand, a study by Sun *et al.* [7] into the ventilation flow in a room, specified that the solution had converged when the energy residuals fell below 10^{-7} and the remainder were below 10^{-4}.

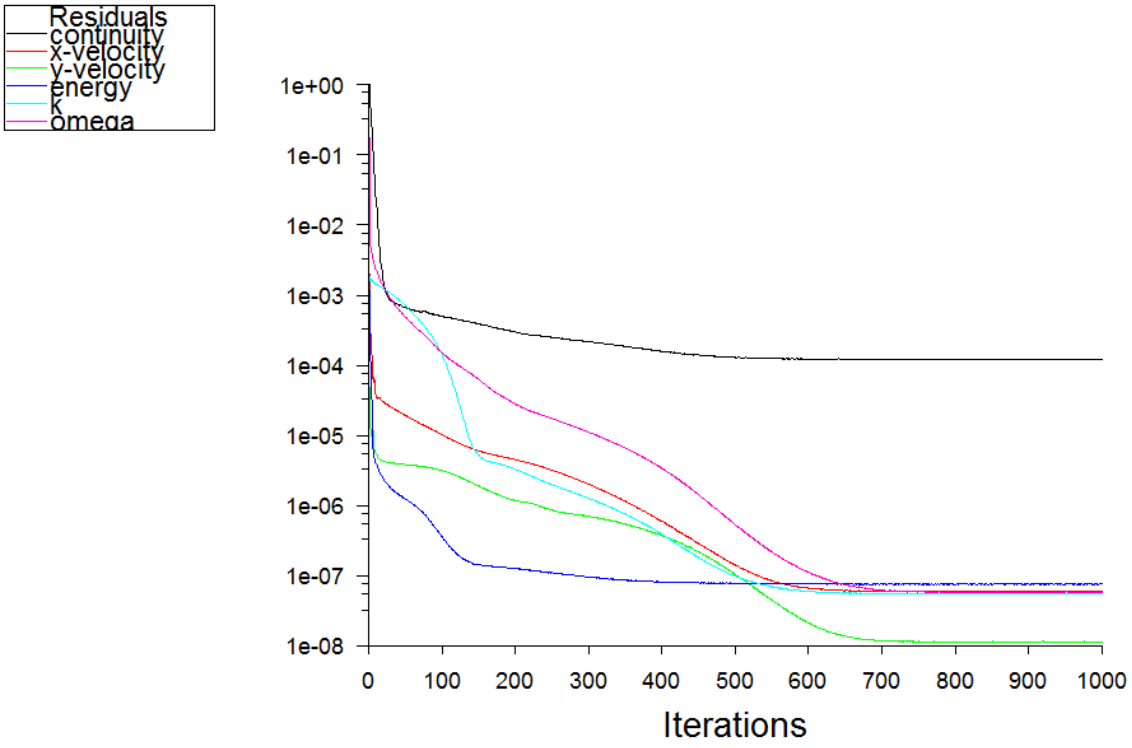

Figure 2.3 – Graph of residuals plotted against iteration number, for a steady-state calculation

3 Methodology

3.1 Project Methodology

ANSYS FLUENT was used to analyse the ventilation flow through the CX501 package. The dimensions for the CFD models were taken from a CAD assembly model provided by Centrax and the models were then created within the ANSYS FLUENT software. The geometry was created using the *DesignModeller* app and then meshed using the *Mesher* app. Finally the case set-up was completed and the calculations were run using the *Fluent* app. This project started with a simple model which was increased in complexity numerous times in order to produce the final CFD model. The reasons for this were twofold. Firstly, it is commonplace for CFD models to take several hours, and even days to run. Having a simple model that produces a solution quickly enables progress to be made much faster. Secondly, a simple model was also easier to corroborate with theory. The initial models were used to determine various user inputs by comparing the results produced by different inputs to theoretical results. Section 3.2 describes the theory used for model validation.

After running a calculation it was important to check that the solution provided by FLUENT had successfully converged. Certain conserved quantities were checked to see if they were conserved in the solution, such as mass flow rate and energy. Another tool that was employed to check whether a solution had successfully converged was a mesh refinement study (also called a mesh convergence study or mesh independency study). This study involves increasing the global number of elements in the mesh and recording the solution. As the number of elements increases the solution should converge. If the solution does not converge this is an indication that there is a problem with the model.

The original project programme changed considerably throughout the duration of this project. The most significant change to the project programme was the time allocated to create the initial models. On the project Gantt chart (that was created at the start of the project) only four weeks was allocated to create an initial model before moving onto the final models. Also there was a significant amount of time set aside to develop the final models once they had been created. In reality all of the model development was done before the final models were created, and this took far longer than the predicted four weeks. The difference in project plan and project execution was mainly due to a lack of CFD experience. The complexity of the models and the time required to run the models was underestimated. However this did not affect the project outcome, instead the project schedule evolved with the project as experience was gained with CFD.

3.2 Corroboration of FLUENT Models with Theory

The accuracy of the solution provided by FLUENT is ‘at best as good as the physics (and chemistry) embedded in it and at worst as good as its operator’ [6]. It is therefore important to corroborate the results provided by FLUENT with theoretical results as well as experimental results. Calculation of the Nusselt number was used to corroborate FLUENT results with

theoretical results to assess whether FLUENT had correctly resolved the thermal boundary layer on heated surfaces. The total heat transfer rate given by FLUENT was also corroborated with theory.

3.2.1 Nusselt Number

The Nusselt number is a dimensionless number which describes the convection heat transfer that occurs at the surface of the object, for these calculations the object was a smooth flat plate.

The local Nusselt number, Nu, is given as [22]:

Equation 3.1

$$Nu = \frac{hx}{k_f}$$

Where: h – local convection coefficient (W/m^2K)
k_f – thermal conductivity of fluid ($W/m \cdot K$)
x – distance from leading edge of plate (m)

The local heat flux, q'' (W/m^2), is given as [22]:

Equation 3.2

$$q'' = h(T_s - T_\infty)$$

Where: T_s – Temperature of plate (K)
T_∞ - Temperature of fluid in the free stream (K)

Combining Equation 3.1 and Equation 3.2 gives:

Equation 3.3

$$Nu = \frac{q''}{(T_s - T_\infty)} \times \frac{x}{k_f}$$

Equation 3.3 was used to calculate the local Nusselt number using data from FLUENT.

The local Nusselt number for a turbulent boundary layer from theory is given as [22]:

Equation 3.4

$$Nu = 0.0296\,\mathrm{Re}_x^{4/5}\,\mathrm{Pr}^{1/3}$$

Where: Re_x – local Reynolds number
Pr – Prandtl number

Equation 3.4 was used to calculate the local Nusselt number from theory.

3.2.2 Total Heat Transfer Rate

One of the results provided by FLUENT is the total heat transfer rate from a surface and so this information was also compared with theoretical values to assess the accuracy of the FLUENT models.

From theory the total heat transfer rate, q (W), is given as [22]:

Equation 3.5

$$q = \bar{h} A_s (T_s - T_\infty)$$

Where: $\bar{h}$ - average convection coefficient (W/m^{2}K)
A_s - area of plate (m^2)

The average Nusselt number for the entire plate is given as [22]:

Equation 3.6

$$\overline{Nu} = \frac{\bar{h} L}{k_f} = 0.037 \, \mathrm{Re}_L^{4/5} \, \mathrm{Pr}^{1/3}$$

Where: L – length of plate (m)
Re_L – Reynolds number for plate

Combining Equation 3.5 and Equation 3.6 gives:

Equation 3.7

$$q = 0.037 \, \mathrm{Re}_L^{4/5} \, \mathrm{Pr}^{1/3} \frac{k_f}{L} A_s (T_s - T_\infty)$$

Equation 3.7 was used to calculate the total heat transfer rate from theory.

3.3 Health, Safety and Risk Management

The health and safety hazards were identified and a risk assessment form was completed for this project. The main hazard was identified as display screen equipment. Spending long periods of time in front of display screen equipment can cause pain due to bad posture or repetitive strain injury. To mitigate the risk posed by this hazard, care was taken to ensure a correctly positioned workstation (following DSE guidelines provided by the University of Exeter [23]) and regular breaks were taken. The full health and safety risk assessment can be found in Appendix D. Owing to the low-risk environment for this project none of the risks identified required further action.

A project risk assessment was also undertaken at the beginning of this project. Various risks to the project were identified and prioritised by estimating the likelihood and severity of each risk. The full project risk assessment table can be found in Appendix E. This is a copy of the original project risk assessment table which was attached to the Preliminary Report for this project. The three most important risks that were identified were: the model would not mesh

properly, the solution would not converge and that the CFD results would not correspond to experimental results provided by Centrax. In order to eliminate the risk of the model not meshing properly, all model geometry was created using the *DesignModeller* app in FLUENT. This was instead of importing the geometry from CAD software, which commonly causes problems when trying to mesh the model. To minimise the risk that the model would not correspond to experimental results from Centrax, numerous models were compared with theory in order to reduce the effect of computational errors on the model. Finally, a common problem that is experienced when using CFD is that the solution fails to converge. To mitigate this risk this project started with a simple model and the complexity of the model was increased only one the model had successfully converged.

4 Design

4.1 Model Development

The final model was created by starting with a simple 2D model, and then gradually increasing the complexity of the model until the final model was reached. Figure 4.1 below shows all of the models that were created in this project. Not all of the models created will be discussed in this report, only the ones that are of significance.

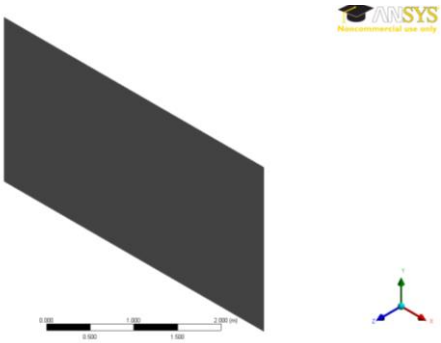

Model 1

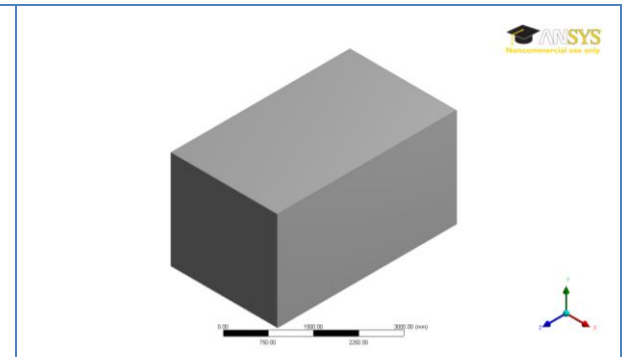

Model 2

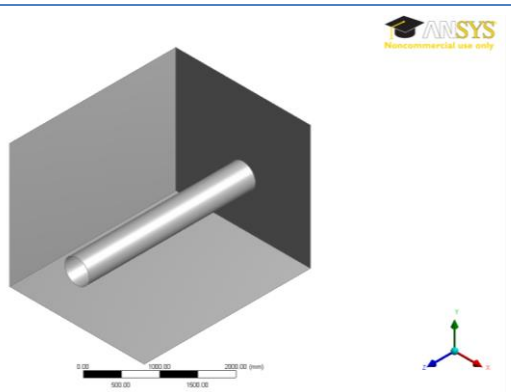

Model 3

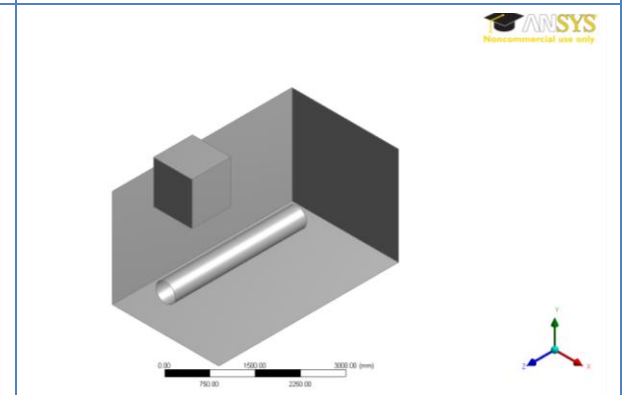

Model 4

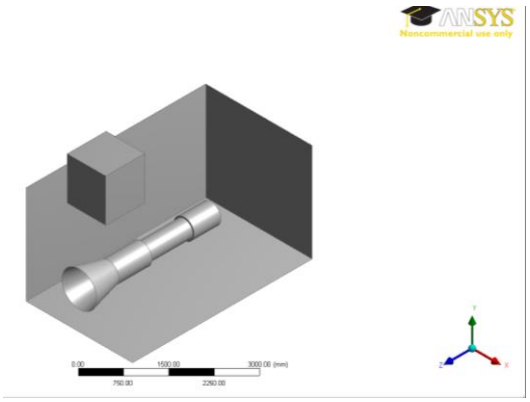

Model 5

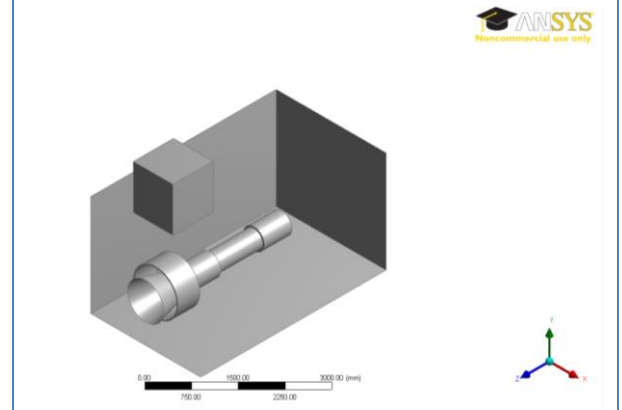

Model 6

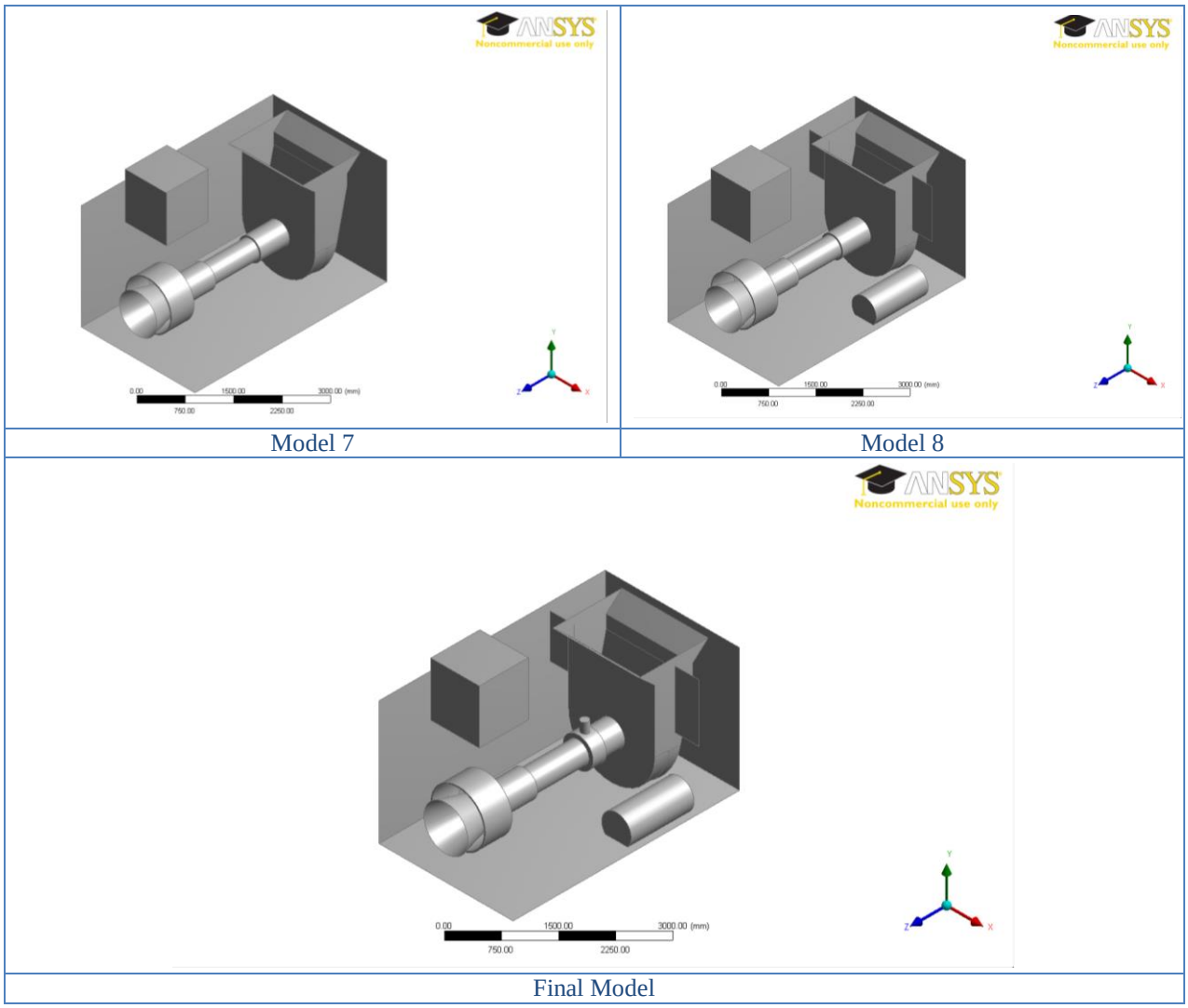

Figure 4.1- Model development

4.2 Model 1

This project started with a simple 2D model of two flat plates in parallel with approximately the same dimensions and fluid properties as the actual domain of the CX501 package ventilation (see Figure 4.2). To calculate the inlet velocity of air, the volumetric flow rate of the fan (9.7 m^3/s) was divided by the inlet area of the model. As the CFD model is only modeling the hazardous area of the package, the model inlet is in the middle of the actual package. The area is approximately 5.7 m^2; which gave an inlet flow speed of 1.7m/s. For a 2D flat plate, a velocity of 1.7 m/s results in a transitional flow in the model. To calculate whether the flow through the CX501 package was laminar, transitional or turbulent, Equation 4.1 was used to evaluate the Reynolds number. The Reynolds number is a dimensionless quantity and is the ratio of a fluids viscous forces to inertial forces. For a non-circular cross-sectional area the Reynolds number is given as:

Equation 4.1

$$R_e = \frac{v d_h}{\mu} \qquad d_h = 4 \times \frac{A}{P}$$

Where: v – velocity of fluid (m/s)
d_h – hydraulic diameter
μ - dynamic viscosity (kg/m·s)
A – cross sectional area (m^2)
P – wetted perimeter of cross sectional area (m)

If R_e < 2,300 then the flow is laminar, if 2,300 < R_e < 4,000 then the flow is transitional and if R_e > 4,000 then the flow is turbulent. Using a velocity of 1.7 m/s, a hydraulic diameter of 2.39 and a dynamic viscosity of 1.983×10^{-5} kg/m.s this gave a Reynolds number of 205,000. The Reynolds number indicated that the flow through the package was turbulent. Hence for Model 1 the inlet air speed was then set to 5 m/s, which is faster than the average air speed through the CX501 package, to ensure that the flow was turbulent and not transitional.

In order to determine the user inputs the initial model was run numerous times using different settings. All calculations were run as steady-state, as this is an 'adequate basis for demonstration of ventilation effectiveness' [9]. When the model had converged (which was when the residuals were around 1×10^{-4} for continuity and below 1×10^{-7} for energy, k, ε and velocity) the results were compared with theoretical results.

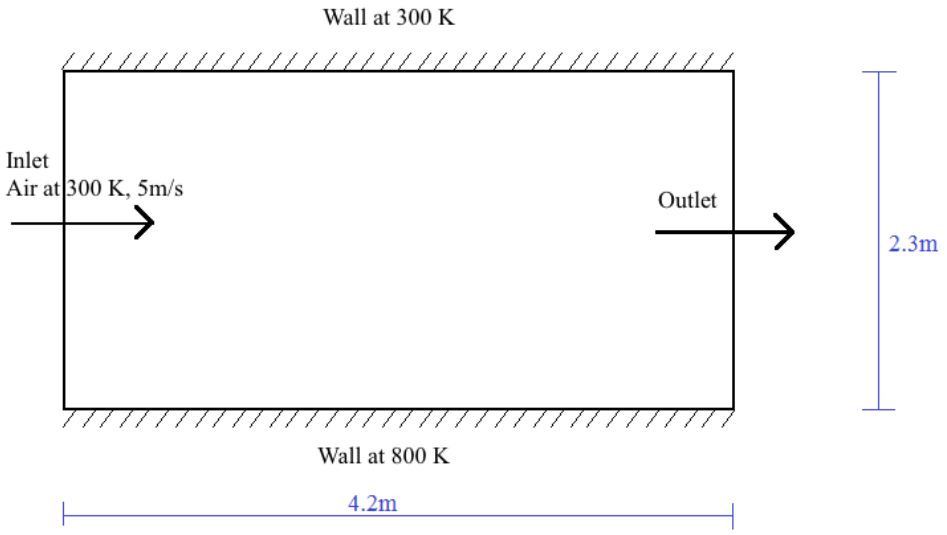

Figure 4.2 – Model 1: 2D two flat plates

4.2.1 Heat Transfer

The energy equation was turned on in order to model the heat transfer from the hot plate.

4.2.2 The Solver

It was not initially evident which solver to use for the CX501 package ventilation. Generally the pressure based solver is used for incompressible, low speed flow, whereas the density based solver is used for compressible, high speed flow. The flow through the CX501 package is low speed (~ 1.7 m/s) but because of the high heat transfer from the gas turbine engine to the ventilation air it could be modeled as compressible. In order to determine which solver to use, Model 1 was run using the pressure based and the density based solver. Running the calculation with the density based solver yielded an unusual temperature profile. The pressure based solver yielded a gradually increasing thermal boundary layer on the hot plate and converged a lot quicker than the density based solver. The rest of the calculations were therefore performed using the pressure based solver.

4.2.3 Viscous Heating Effects

The Brinkman number is a dimensionless number important in heat transfer by conduction in viscous liquids, it is defined as:

Equation 4.2

$$B_r = \frac{\mu v^2}{k\Delta T}$$

Where: μ - dynamic viscosity (kg/m·s)
v – velocity of fluid (m/s)
k – thermal conductivity of fluid (W/m·K)
ΔT – temperature difference between the fluid and the wall (K)

When the pressure based solver is used, the effect of viscous dissipation is not included as it is normally negligible in incompressible flows. Viscous dissipation terms can be included in the pressure based solver by turning on viscous heating effects. Viscous heating will only be important when the Brinkman number (as defined in Equation 4.2) is greater than, or equal to 1 [18]. In this case the Brinkman number is much less than 1 and so viscous heating effects were not included in the pressure based solver.

4.2.4 Buoyancy Effects

The effect of buoyancy on the CX501 package ventilation flow is non-trivial and FLUENT has several different ways of modeling buoyancy. One method involves using the Boussinesq approximation, the basic principle of which is that ‘variations of density can be ignored except where they are multiplied by the acceleration of gravity in equation of motion for the vertical component of the velocity vector’ [24]. A calculation was run for Model 1 with the Boussinesq model turned on, and the local Nusselt number was calculated at numerous

locations along the plate using the results from FLUENT and Equation 3.3. The local Nusselt number was also calculated from theory using Equation 3.4. Figure 4.3 is a graph of the local Nusselt number plotted against the local Reynolds number at over 150 locations along the plate, thus giving the appearance of a smooth line for the FLUENT calculations. Figure 4.3 shows that using the Boussinesq model, the thermal boundary layer was not correctly resolved by FLUENT and so it was not used in further calculations.

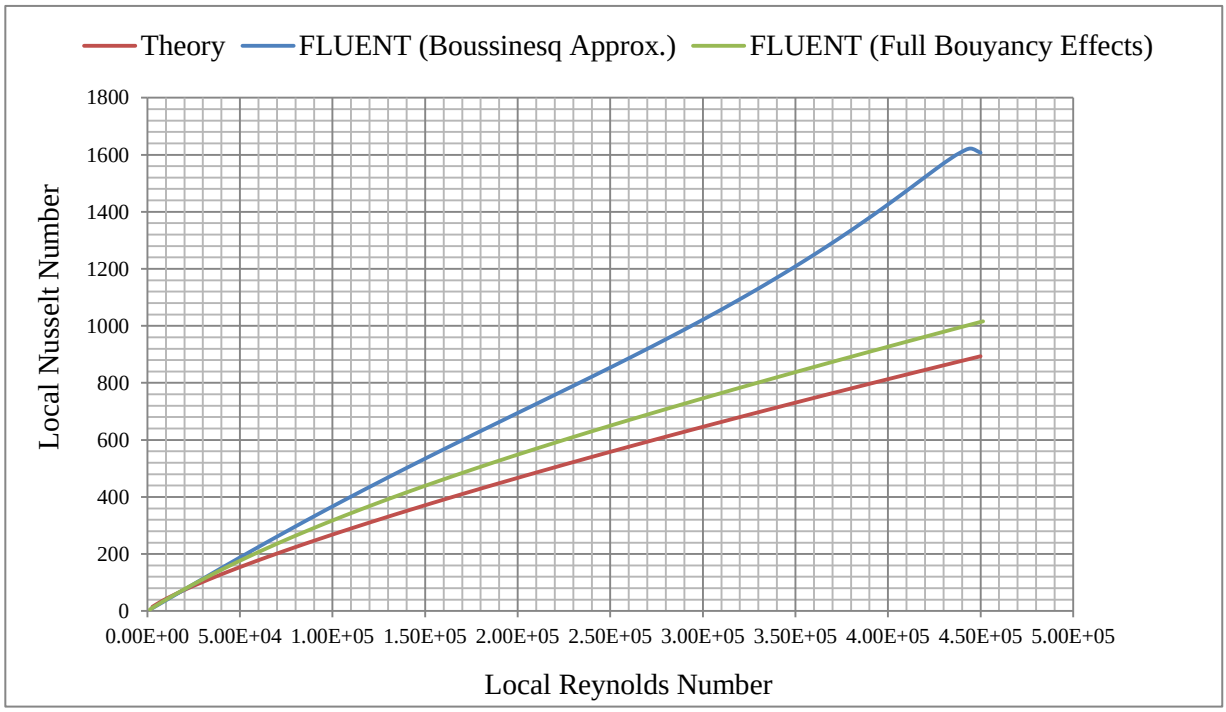

Figure 4.3 – Local Nusselt number plotted against local Reynolds number for Model 1

Another method used to account for buoyancy is to apply a non-zero gravity force in a non-isothermal flow. This ensures that buoyancy is included in the k part of the k-ε turbulence model. Buoyancy effects also then need to be included in the ε term; known as applying full buoyancy effects. Once implemented, the results showed a much better agreement with theory as shown in Figure 4.3.

4.2.5 Mesh Refinement Studies

Using the pressure based solver with full buoyancy effects, a mesh refinement study was carried out to assess whether the solution had converged. Figure 4.4 is a graph of total heat transfer rate plotted against the total number of elements in the mesh. This graph shows that as the number of elements in the mesh increases, the solution converges at around 37.8 kW. Theoretical heat transfer rate calculated from Equation 3.7 gives the total heat transfer rate as 34.2 kW, hence the results provided by FLUENT deviate by around 10% from theory. Further investigation into the mesh was carried out to try and improve the accuracy of the value provided by FLUENT.

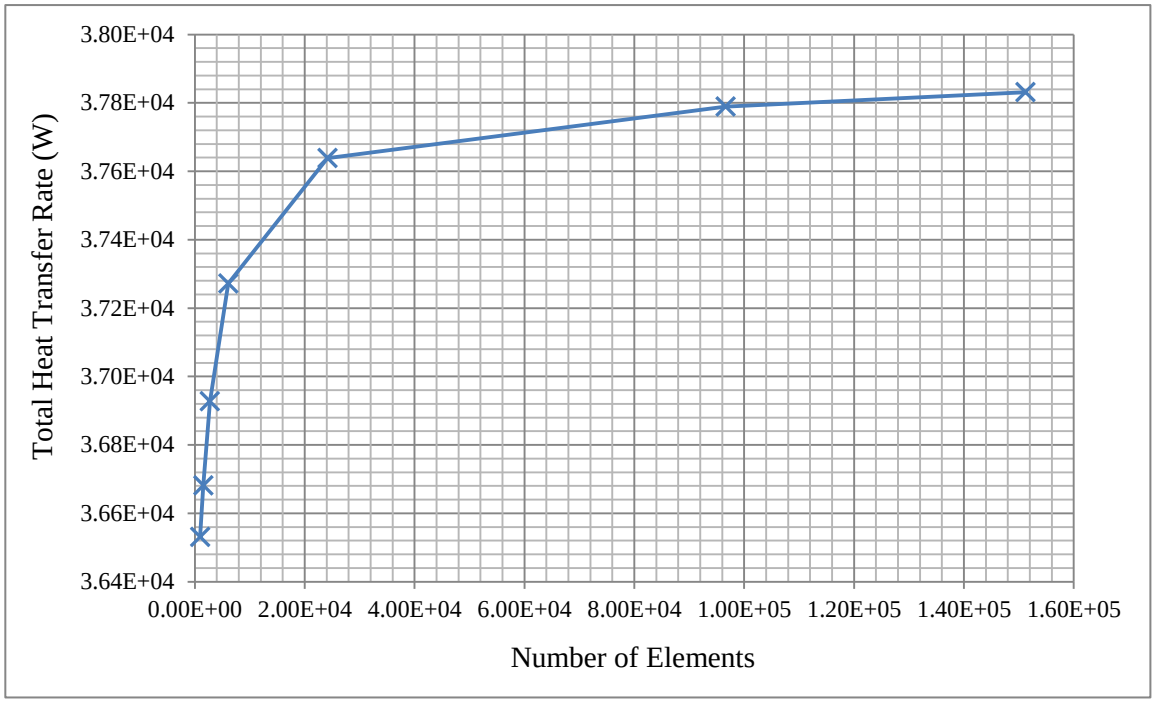

Figure 4.4 – Mesh refinement study for Model 1

The local Nusselt number was calculated along the plate for the coarsest and finest mesh (966 elements and 151,000 elements respectively) using Equation 3.3. This was then plotted against the local Reynolds number and compared with theoretical results calculated using Equation 3.4 (a graph of the results is in Appendix A, Figure A.1). It was found that increasing the number of elements in the mesh had very little effect on the accuracy of the local Nusselt number. The second part of the mesh refinement study was to perform a local refinement on the hot plate. Using a global element size of 0.02m (which gave around 26,000 elements in total) the number of elements in the mesh around the hot plate was increased using a refinement factor of 0, 1, 2 and 3. Increasing the local refinement on the hot plate had a much greater effect on the accuracy of the local Nusselt number as shown in Figure 4.5. The local Nusselt number was calculated at over 200 points along the plate, thus giving the appearance of a smooth line for the FLUENT calculations. A mesh with a total number of 28,875 elements, including a refinement factor of 3 around the hot plate, resulted in a total heat transfer rate of 35.2 kW. This was deemed a satisfactory solution, as it was only a 3% deviation from theoretical results.

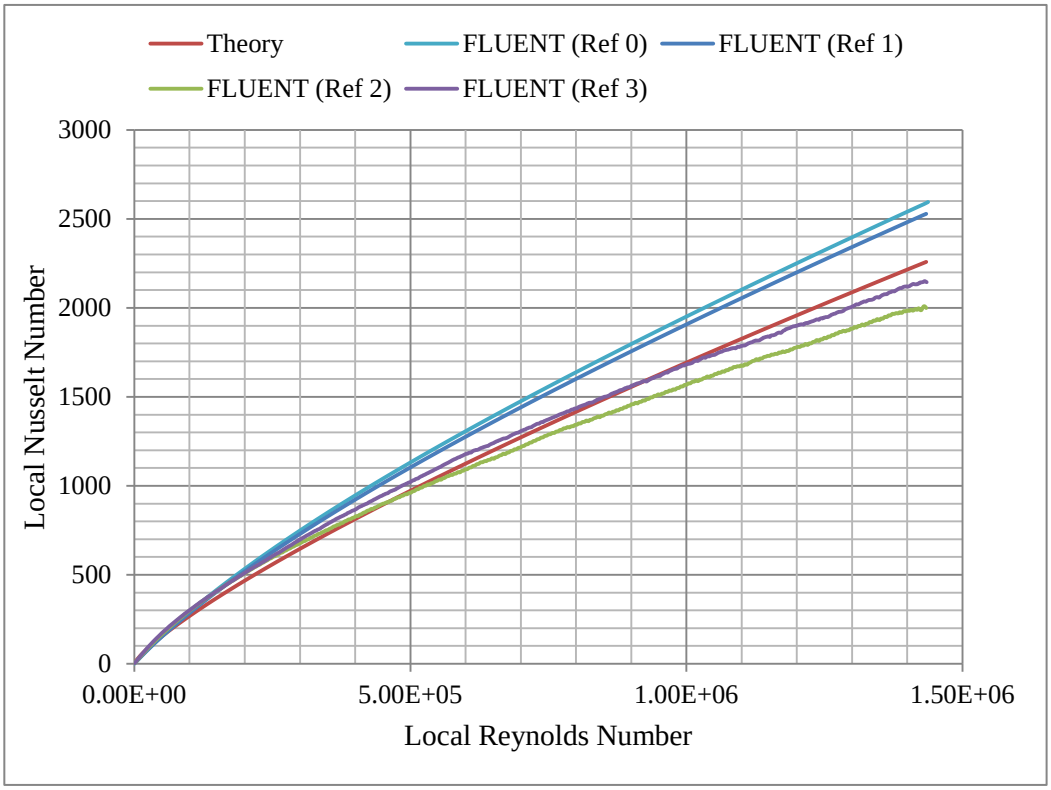

Figure 4.5 – Local Nusselt number plotted against local Reynolds number with refinement factor of 0, 1, 2 & 3 around the hot plate.

4.2.6 Turbulence Models

Once the model had been corroborated with theory, an investigation into different turbulence models was performed. Four different turbulence models were investigated for Model 1; k-ε, RNG k-ε, k-ω and SST k-ω. These models were chosen as they were the four most common models used in studies that were investigated in the literature review. For these turbulence models the turbulence was specified using an intensity of 10% and a length scale of 0.1m. The local Nusselt number was plotted against the local Reynolds number and the results for the three turbulence models were compared with theory (see Figure A.2 in Appendix A for graph of results). The results revealed that there was no difference between the k-ε and k-ε RNG models or the k-ω and SST k-ω models. The results also indicated that the k-ε turbulence models provided more accurate results than the k-ω models. The rest of the calculations were therefore performed using the standard k-ε turbulence model.

4.3 Model 3

The third model that was created was a 3D model of a hot cylinder inside a rectangular prism, as shown in Figure 4.6. The model was meshed with a total of 636,294 elements including a refinement factor of 2 around the cylinder. The calculation was run using: the pressure based

solver, the k-ε turbulence model, full buoyancy effects and the energy equation. The inlet flow speed was set at 1.7 m/s.

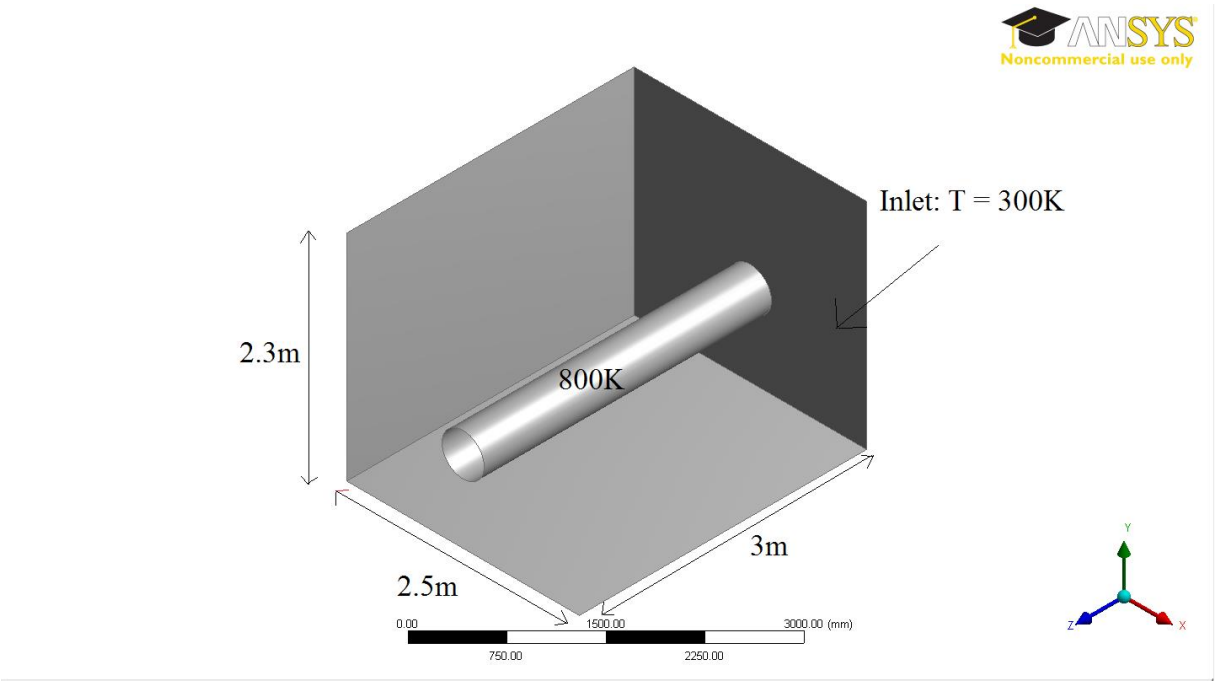

Figure 4.6 – Model 3: 3D cylinder inside rectangular prism

The results from FLUENT gave a total heat transfer rate from the cylinder of 13.8kW. Reliable theoretical calculations of heat transfer from a cylinder in axial flow were not found. Consequently to calculate theoretical results, the cylinder was assumed to be a flat plate and Equation 3.7 was used. Using Equation 3.7 gave a total heat transfer rate of 15.9 kW. A mesh refinement study on the initial 3D model indicated that the solution was converging to a value below the expected theoretical value. As the total heat transfer rate calculated by FLUENT for Model 1 was an overestimate, this suggested that the thermal boundary layer around the cylinder had not been correctly resolved. To try and resolve this problem, the mesh around the cylinder was investigated.

4.3.1 Boundary Layer Meshing

Using the inflation tool, a boundary layer mesh was applied to the turbine as shown in Figure 4.7. The boundary layer mesh was adjusted to ensure that the y^+ and the y* values were within an acceptable range; $20 < y^+ < 200$ [9] and $y^* > 11.225$ [18]. A mesh refinement study was then performed on this model (see Figure 4.8), the results indicated that the solution was converging to a value of around 17 kW. This value is 7% higher than the theoretical results calculated using Equation 3.7, however this equation is for a flat plate not a cylinder. A study by Lee *et al.* [25] into the effect of convex curvature on heat transfer, found that as the length to diameter ratio of a cylinder increases, so does the difference in heat transfer from the same flow conditions over a flat plate. It also revealed that 'in all cases the friction coefficient is always greater (for a cylinder) than that of a flat plate'. Therefore the total heat transfer rate

calculated by FLUENT should be greater than the value calculated using Equation 3.7, thus the results provided by FLUENT were deemed satisfactory.

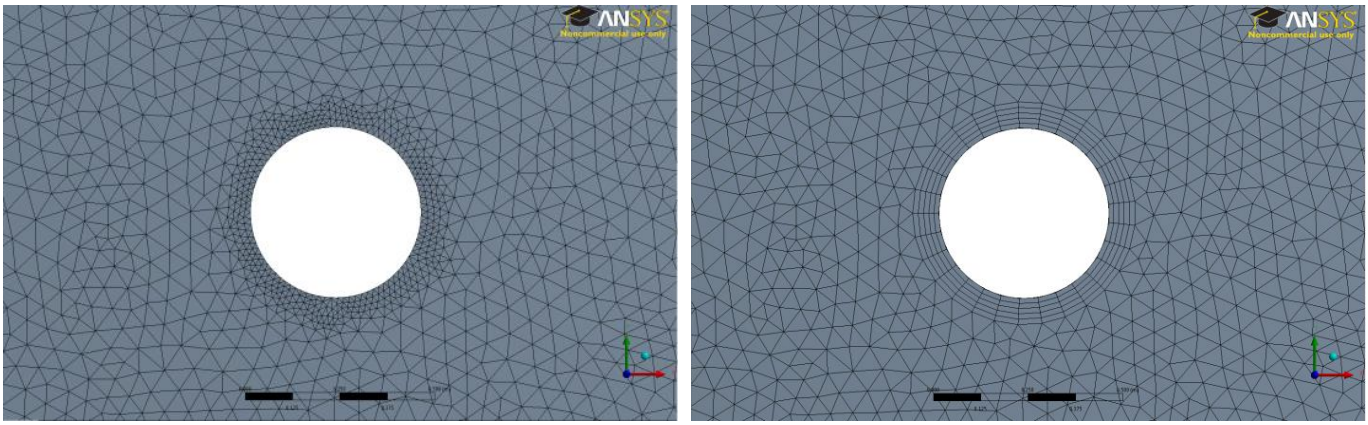

Figure 4.7 - Model 3 showing refinement factor 2 around cylinder (on the left) and a boundary layer mesh around cylinder (on the right)

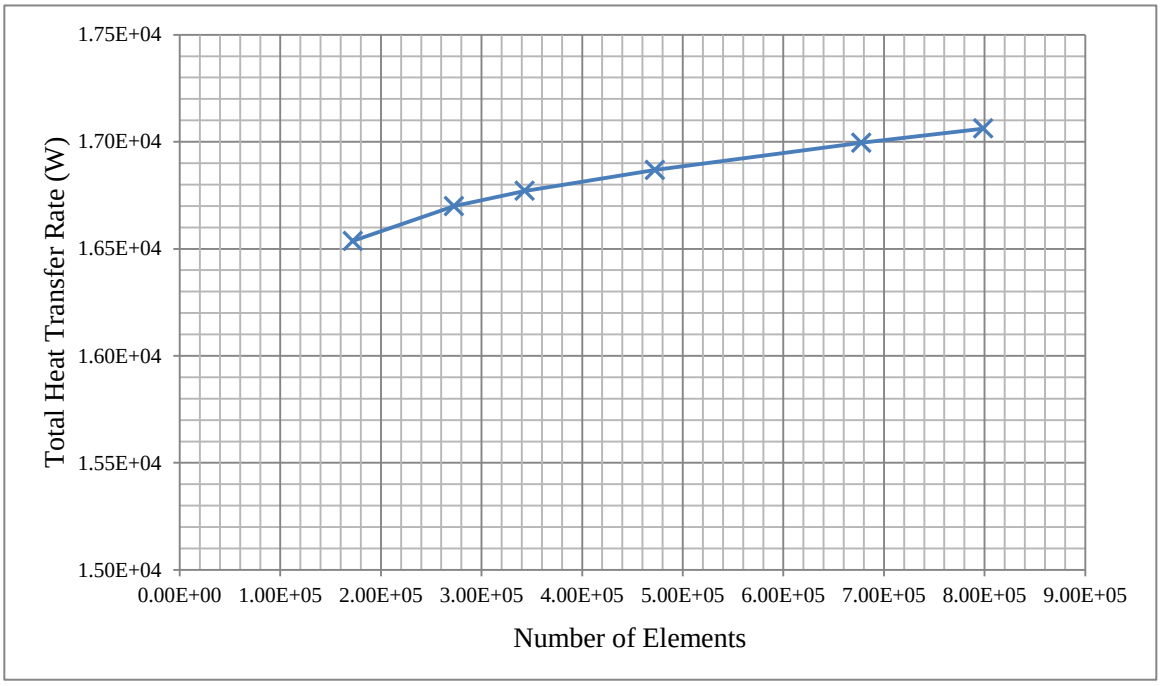

Figure 4.8 – Mesh refinement study on Model 3

4.4 Model 5

Model 5 was the first model where the gas turbine engine was modeled more like its actual shape, rather than been modeled as a cylinder. It was this model where the graph of residuals started to portray signs of instability. In a steady-state calculation, the graph of residuals should show the residuals dropping and then leveling out (in a similar fashion to the graph of

residuals shown in Figure 2.1). However with Model 5, after initially dropping, all the residuals showed significant fluctuation and residuals for continuity remained relatively high (around 1×10^{-2}), as can be seen in Figure 4.9. A detailed investigation was then carried out to determine the source of instability and involved altering numerous features of the model one at a time and assessing the residuals to locate the cause of the instability. If for example, the model converged with a finer mesh, the source of instability would be with the mesh. Firstly, the energy equation was turned off and the calculation run as cold-flow. The mesh was then refined around the gas turbine engine and the number of elements in the mesh was increased. After this, different values for intensity and length scale in the turbulence model were used, and different turbulence models were tried. Finally, alternative wall treatments were applied - yet none of these measures improved the convergence of the model.

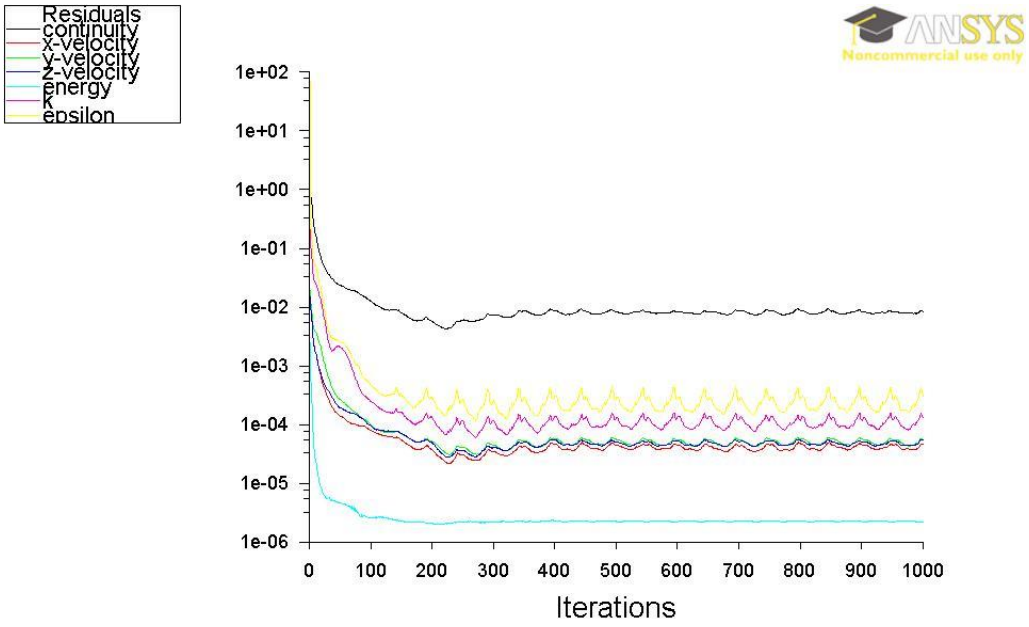

Figure 4.9 – Graph of residuals for Model 5 when running a steady-state calculation

The preceding model (Model 4) had run successfully under identical flow conditions and the only difference between the models was the model geometry. Whereas Model 4 had a simple cylinder modeling the gas turbine, Model 5 had a shape that more resembled the geometry of the gas turbine engine. The problems with the residuals could not be attributed to the case set-up, so it was believed that although the flow through the package as a whole was steady-state, there was some periodic characteristic of the flow which was affecting the convergence of the model. This periodic characteristic was most likely vortex shedding or eddy formation, caused by the change in geometry of the gas turbine. The next step in the process was to run a transient calculation.

4.4.1 Transient Calculations

4.4.1.1 Courant–Friedrichs–Lewy Condition

When running transient calculations special consideration was given to the Courant-Friedrichs-Lewy condition. The Courant-Friedrichs-Lewy condition is defined as [26]:

Equation 4.3

$$C = \frac{u\Delta t}{\Delta x} \leq C_{\max}$$

Where: C – Courant number
u – velocity (m/s)
Δt – time step (s)
Δx – length interval of mesh (m)

The value of C_{max} depends on the solver used - if an explicit solver is used then $C_{max} = 1$, but implicit solvers can handle values of C_{max} that are much greater than 1 [26]. This project used the pressure based solver, which can only use implicit formulations of the solver. Therefore it would be possible to run a transient calculation with a cell Courant number greater than 1, however this signifies that in one time step the solution skips one or more elements within a mesh. Similarly, a Courant number of 0.5 means that there are two time steps within an element of the mesh. Consequently, it is good practice to have an average cell Courant number less than 1. Therefore all transient calculations were run using a Courant number of less than 1.

4.4.1.2 Solution Algorithms SIMPLE vs. PISO

All of the calculations that had been run up to Model 5 were run as steady-state using the SIMPLE algorithm. The algorithm is the numerical procedure used to solve the Navier-Stokes equations. SIMPLE (Semi-Implicit Method for Pressure-Linked Equations) is the default algorithm on FLUENT. When running transient flow calculations the PISO (Pressure-Implicit with Splitting of Operators) algorithm is highly recommended [27]. Both SIMPLE and PISO are pressure-velocity coupling algorithms, where 'the fundamental concept . . . is to derive a pressure correction equation by enforcing mass continuity over each cell' [28]. The SIMPLE algorithm is a trial and improvement method for solving the Navier-Stokes equations sequentially starting with an initial estimate of pressure. The PISO algorithm is similar to the SIMPLE algorithm but it has two additional correction steps. This enables faster convergence (especially for transient calculations) and better results for highly skewed meshes. Further details on pressure velocity coupling algorithms can be found in *An introduction to computational fluid dynamics: the finite volume method* by H.K. Versteeg, and W. Malalalsekera [5]. The following transient calculations were then run using the PISO algorithm.

4.4.1.3 Transient Results

Model 5 was subsequently run as a steady state calculation for 1,000 iterations and then as a transient calculation with time step of 0.01 which gave a volume average cell Courant number of 0.8.

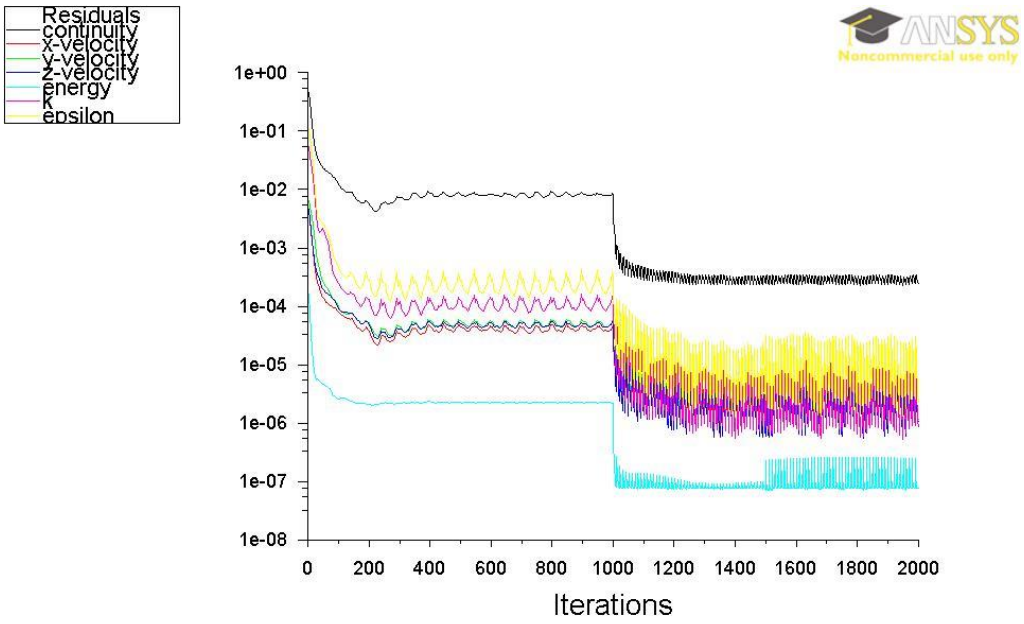

Figure 4.10 – Graph of residuals for Model 5 running a steady-state and then transient calculation

Figure 4.10 is the graph of residuals for Model 5 running a steady-state and then transient calculation. When running a transient calculation the residuals are expected to decrease and then level out while oscillating as shown in Figure 4.10. The graph of residuals indicates that running a transient calculation has improved the solution of Model 5, as all the residuals have decreased in value.

5 Results & Analysis

5.1 Final Model

5.1.1 Geometry

The geometry of the final model is shown in Figure 5.1. In addition to the gas turbine engine, large objects that will significantly affect the package ventilation flow have also been included in the model. The bottom face of the model is where the tread plate is located on the CX501 package. The tread plate is a grated surface that can be stood on in order to carry out maintenance; underneath the plate there is a dense network of pipes including gas pipes. As the tread plate is not a wall, a symmetry boundary condition has been applied to this face, effectively imposing a slip condition.

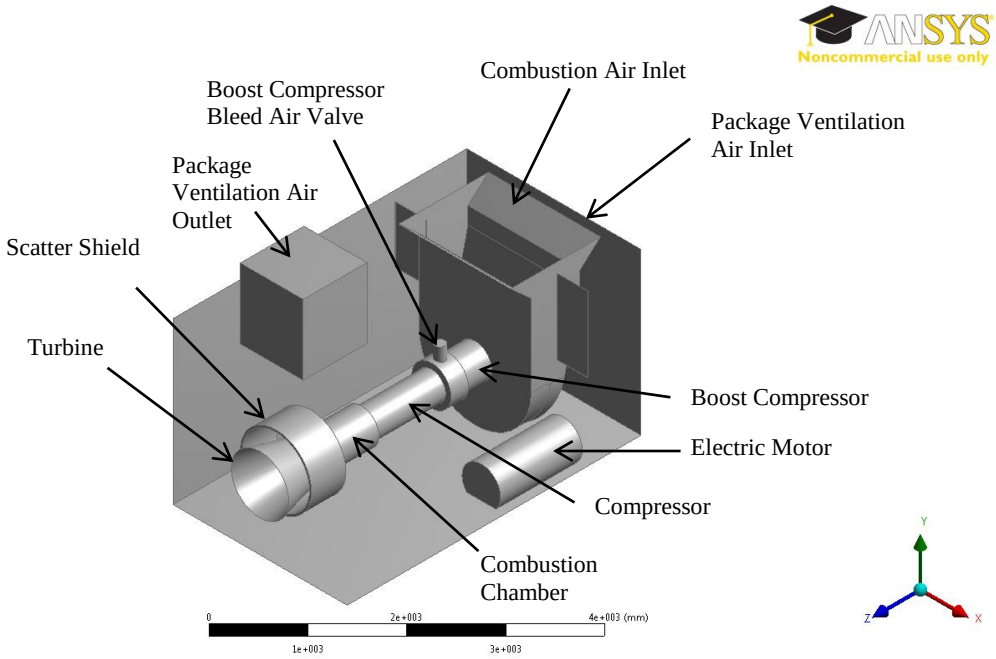

Figure 5.1 – Geometry of final model

5.1.2 Mesh

A mesh refinement study was carried out on this model; the number of elements in the mesh was increased and the total outlet temperature recorded (see Figure 5.2 for a graph of the results). This mesh refinement study indicates that the outlet temperature is converging to around 312K. From these results a mesh of around 500,000 elements for the final models was deemed a suitable compromise between accuracy and time.

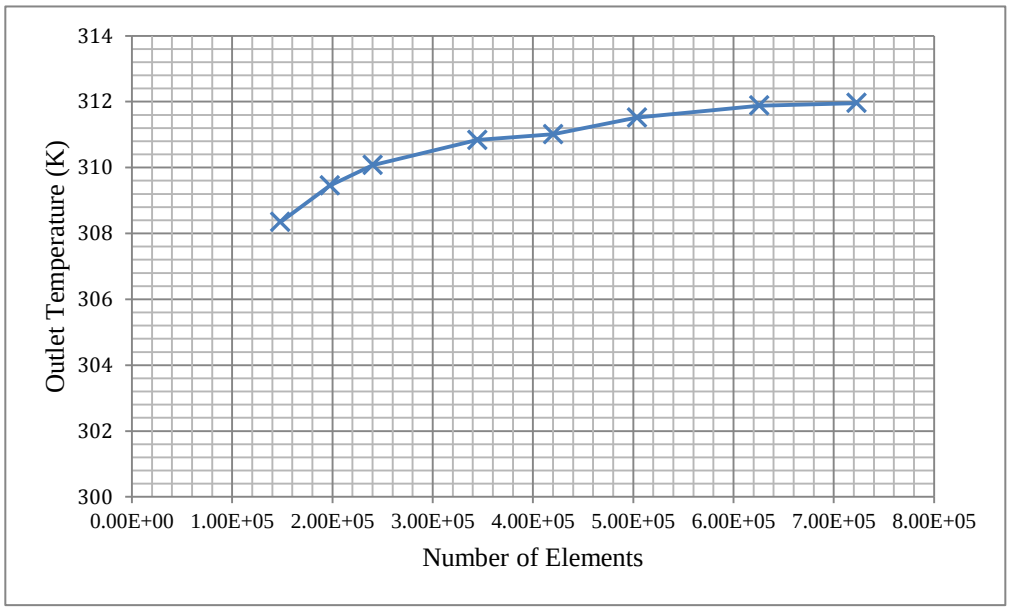

.

Figure 5.2 – Mesh refinement study for final model

The mesh for the final model can be seen in Figure 5.3. This is a cross section of the mesh on the y-z plane which bisects the model. The final model was meshed with 509,950 elements and a boundary layer mesh around the gas turbine engine. Figure 5.4 shows the boundary layer mesh that was applied to the gas turbine engine and scatter shield.

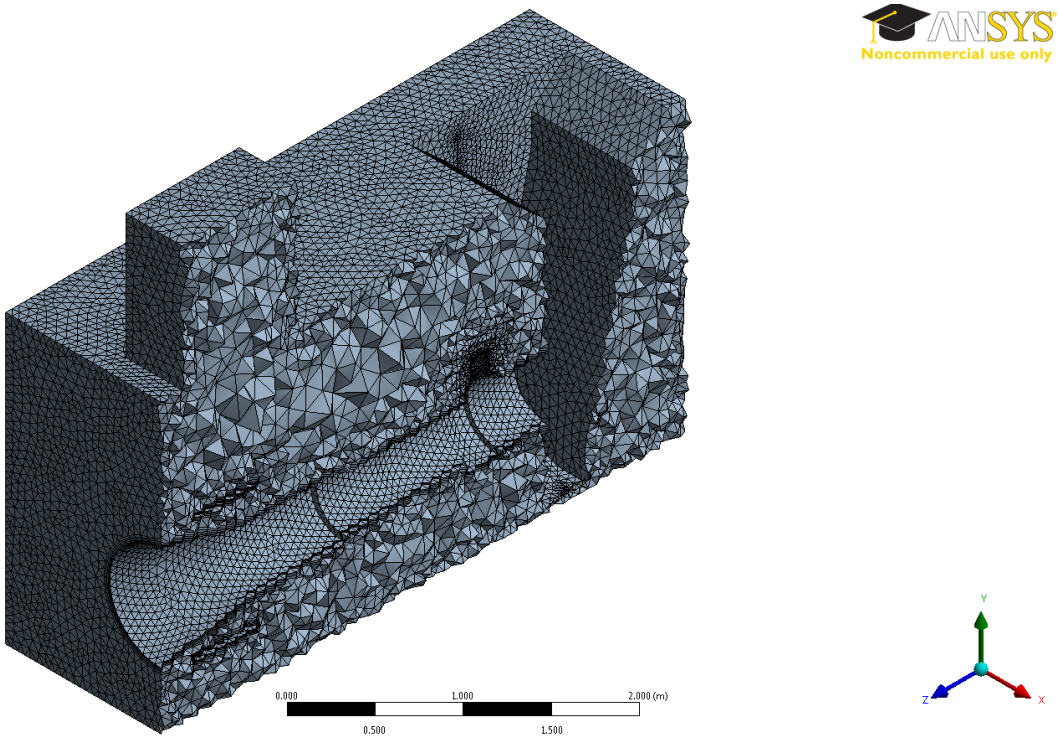

Figure 5.3 – Cross section of the meshed used for the final models

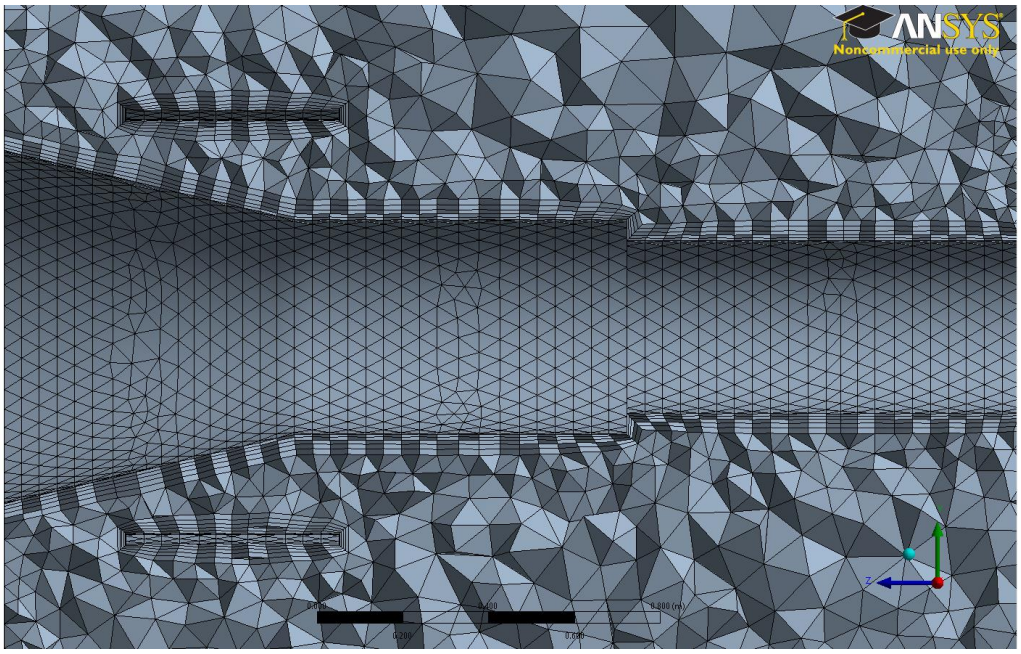

Figure 5.4 – Cross section of the mesh showing boundray layer mesh

When considering the mesh, it is the quality as well as the quantity of cells that is important. The cell orthogonal quality and cell skewness were checked for this mesh. The best cells will have an orthogonal quality close to 1 [29]. Figure 5.5 indicates that most of the cells have an orthogonal quality greater than 0.6 - the volume-weighted average cell quality is 0.86. The equivolume skew of a cell is a measure of the difference between the cell and an equilateral cell of equivalent volume. Values for equivolume skew should be no more than 0.95, with an average value of significantly lower [29]. Figure 5.6 indicates that most cells in the mesh have an equivolume skew of less than 0.6 - the volume-weighted average for the mesh is 0.23. These results indicate that the elements in the mesh are of good quality.

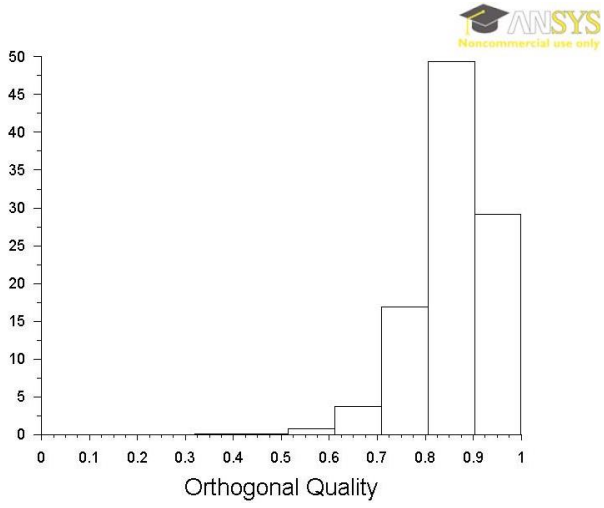

Figure 5.5 – Histogram of orthogonal quality

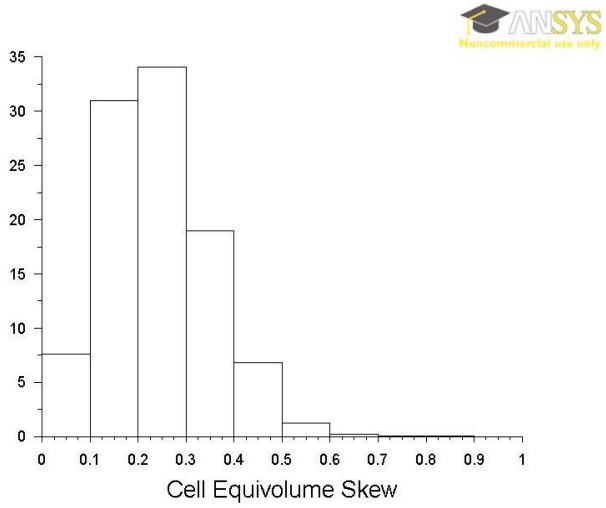

Figure 5.6 – Histogram of cell equivolume skew

5.1.3 Comparison with Experimental Results

In order to assess the validity of the model it was compared with data provided by Centrax from a test on the CX501 package. The package was run for 3 hours under normal operating conditions. The ambient air temperature outside the package was 7°C (280K) and the ventilation fan was running at 9.7 m^3/s. Under these conditions the ventilation air temperature at the outlet of the package was measured as 42°C (315K). The CFD model was run under similar conditions, in order to compare results. As the CFD model only represents the hazardous area of the package, the temperature of the air at the inlet to the model is higher than the ambient air temperature. This is because the air is heated as it flows past the generator (in the non-hazardous area of the package). On a long run (of 3-4 hours) and with an ambient air temperature of 7°C, the rise in air temperature from the generator is around 20°C. Therefore the model was run with an inlet temperature of 27°C (300K) and an inlet mass flow rate of 11.4 kg/s.

Initially the results provided by FLUENT gave an average outlet temperature of 308.5K. This was 6.5K lower than the experimental results for the package. As the temperatures for the surfaces of the gas turbine engine had been taken from experimental in-situ results, it was deemed that the discrepancy was probably due to the surface of the gas turbine engine being modeled as smooth. In reality the surface is not smooth, and has many objects such as pipes, flanges and fittings protruding from its surface. Heat transfer from forced convection is greater for rough surfaces than it is for smooth ones, as 'surface roughness affects the wall-fluid heat and mass transfer by increasing the total interfacial area and, more important, by causing local mixing of the fluid' [30].

To try and increase the accuracy of the model a wall roughness was applied to the surfaces of the gas turbine engine. FLUENT allows the user to input two values when specifying wall roughness; the roughness constant and the roughness height. The default roughness constant was used (0.5) as 'a clear guideline for choosing [the roughness constant] for arbitrary types of roughness is not available' [31]. In order to determine the roughness height, a study was done on Model 1. The roughness height applied to the hot wall was increased and the outlet temperature measured. The results in Figure 5.7 demonstrate that increasing the wall roughness height increased the temperature of the air at the outlet of the model. However, at a roughness height of around 0.005m the results show that the outlet temperature has plateaued - this was the expected result. At a wall roughness height of 0.005m the surface is 'fully rough' and so increasing the roughness no longer has an effect on the heat transfer. Prior to Version 14 of FLUENT, care had to be taken to ensure that the wall roughness height was not greater than the height of the wall adjacent cell. However, the rough wall formulation used in FLUENT 14.2 'eliminates all restrictions with respect to mesh resolution near the wall, and can therefore be run on arbitrary fine meshes' [31].

Using this information, the wall roughness function was applied to all heated surfaces using a roughness coefficient of 0.5 and a roughness height of 0.005m. The calculation was re-run and the results provided by the model gave an average outlet temperature of 311.4 K; 3.6K less than the experimental results. Different surface roughness values were tried, but it was found that increasing the roughness height beyond 0.005m did not increase the outlet temperature.

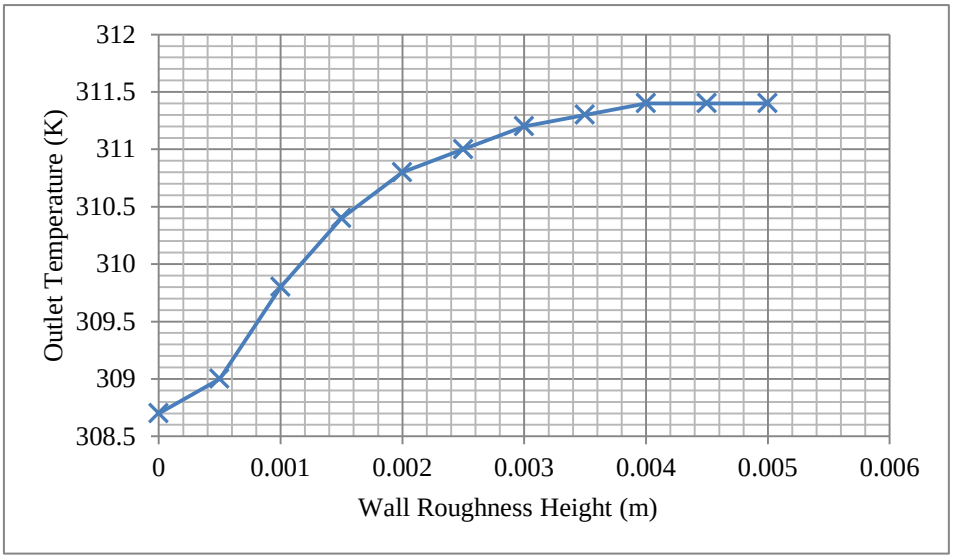

Figure 5.7 – Graph of outlet temperature plotted against wall roughness for Model 1

Despite increasing the surface roughness the outlet temperature of the model was still slightly less than the experimental value. This discrepancy is most likely down to physical inconsistencies between the CFD model and the actual CX501 package, rather than computational errors within the model. The wall roughness function uses a sand grain model, where the roughness height is equivalent to the height of a grain of sand on the surface of the model. In actual fact the surface of the gas turbine, which has pipes and other objects covering its surface, will have a far greater impact on the surrounding airflow than a surface modeled with a sand grain wall roughness.

5.1.4 Boundary Conditions

5.1.4.1 CX501 Model without Bleed Air

After comparison with experimental results the next step was to apply specific environmental conditions to the model. Centrax wanted the models to be run using 'worst case scenario' environmental conditions. This was specified as Russia on a very hot day; with an ambient temperature of 40°C, and with the outlet fan running at a volumetric flow rate of 9.7m^3/s. As mentioned, the air at the model inlet is higher than ambient air temperature as it is heated as it flows past the generator. At an ambient temperature of 40°C, the CX501 generator will be running at a maximum of 2.5 MW and experiencing heat losses of 2.5%. To calculate the temperature rise of the air as it heated by the generator, Equation 5.1 was used:

Equation 5.1

$$\dot{Q} = \dot{m} c_p \Delta T$$

Where: $\dot{Q}$ - heat transfer rate (W)
$\dot{m}$ - mass flow rate (kg/s)
c_p - specific heat capacity (J/kgK)
ΔT - temperature rise

Using $\dot{Q}$ as 62.5 kW (2.5% of 2.5 MW), $\dot{m}$ as 11kg/s (9.7 $m^3/s \times 1.13$ kg/m^3) and c_p as 1.005 kJ/kg.K this gave ΔT as 6K. The inlet flow to the model was then set at 46°C (319 K).

Scalable wall functions were applied, primarily because the use of scalable wall functions avoids the need to have the y^+ and y* values of the mesh within a particular range. The temperatures for the surfaces of gas turbine engine and scatter shield were taken from in-situ temperature measurements taken by Rolls-Royce and data given by Centrax. A table of the surface temperatures can be found in Appendix B. These surfaces were set as rough walls using a roughness constant of 0.5, and a wall roughness height of 0.005m. All other wall surfaces in the model were set at the same temperature as the inlet air (319K). This value was chosen because Centrax specified that on a long run, the temperatures of the walls and other surfaces can be approximated to the temperature of the air as it flowed past the combustion air inlet [32]. As the temperatures of the walls and other surfaces were specified there was no need for a radiation model to be used, as discussed in Section 2.2.4.3.

The inlet was set as a mass flow inlet of 11 kg/s to give a volumetric flow rate through the package of 9.7 m^3/s at a temperature of 46 °C (air density 1.13 kg/m^3). The standard k-ε turbulence model was applied and the inlet was specified with an intensity of 10% and a length scale of 0.1m. The outlet was set as a pressure outlet at atmospheric pressure (0 barg) as the package air vents to the atmosphere. Backflow properties were specified for the flow. Turbulent intensity and length scale were set the same as the inlet and the total temperature was set at 10K above the inlet temperature. Backflow properties are specified in order to alleviate the effect of reversed flow at the outlet, which is where the flow reverses in direction at the outlet boundary. The properties of air (such as density and thermal conductivity) were set at constant values, as a study by Defraeye *et al.* [13] found that 'the use of air properties . . . that are temperature dependent did not improve the results significantly.'

5.1.4.2 CX501 Model with Bleed Air

In order to have a comparable model the conditions for the model with boost compressor air bleed were identical to the model without boost compressor air bleed with the exception of 3.7 kg/s of bleed air emitted from the bleed air valve at 348K. Hence the mass flow at the inlet was reduced to 7.3 kg/s to give a total mass flow of 11 kg/s at the outlet. The boost compressor bleed air had a turbulent intensity of 3% and length scale of 0.01m. This was calculated by treating the 5.5" (140mm) valve as a pipe of the same diameter, and using equations for turbulent intensity and length scale given in the FLUENT User Guide [31].

5.1.5 Reversed Flow

After the calculation was run with boost compressor air bleed, the results were showing a high level of reversed flow at the outlet boundary. Reversed flow can cause problems with convergence of the model and affect results. To prevent reversed flow occurring, the outlet was increased by 1m. This does not accurately represent the ducting used at the outlet of the CX501 package but will not have a significant effect on the results. In order to have comparable models, the outlet was increased on the model without boost compressor air bleed and the calculation was run again.

5.1.6 Calculations

For both models, a steady state calculation was run for 500 iterations and then a transient calculation was run for a total of 5 seconds. The transient calculation was run with a time step of 0.002s and 5 iterations per time step. This gave a volume average cell Courant number of 0.39 for the model without boost compressor air bleed, and 0.93 for the model with boost compressor air bleed. All of the residuals for both models fell below 1×10^{-3} and a graph of the residuals for the model without boost compressor air bleed can be seen in Appendix C (this was very similar to the graph of residuals with boost compressor air bleed). For the transient calculations the solution was saved every 0.5s and the outlet temperature was plotted against time (Figure 5.8 is a graph of the results for both models). This graph shows that the outlet temperature fluctuates slightly with time but overall there is little change (all results were +/- 0.3% of the average temperature). This is what was expected for this calculation as it is a steady state calculation with some transient behavior, thus the outlet temperature should not change significantly with time.

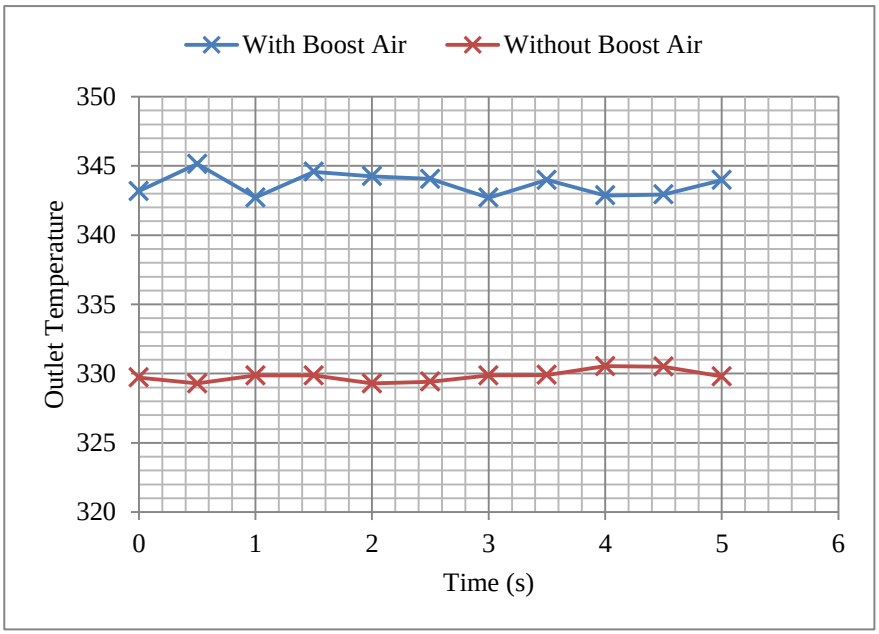

Figure 5.8 – Graph of outlet temperature plotted against time for the final models

5.2 Presentation of Results

One of the main objectives of this project was to assess the effect of adding boost compressor air bleed to the CX501 package ventilation by comparing the two CFD models. In order to facilitate easy comparison of the models, the results from both models will be analysed by presenting them adjacent to each other. The two primary functions of the CX501 package ventilation are: to cool the air inside the package and to provide sufficient airflow to disperse any potential gas leaks. Considering this, the results are compared with special interest given to the velocity and temperature of airflow inside the package. Various pictures of results are included in this report which will adequately display the ventilation flow, however the files for

the final model on a CD have been attached to the back cover of this report should the reader wish to study the results further. These files can only be opened on a computer running ANSYS FLUENT.

5.3 General Package Flow

Figure 5.9 shows the velocity vectors for the model without boost compressor air bleed. The velocity vectors show that as the air flows past the combustion air inlet, the air is accelerated over and underneath the side panels and is then drawn up through the outlet. This motion causes two large eddies to form either side of the gas turbine. The scale on this picture is 0 to 20m/s and the average air velocity in the package is 4.1 m/s.

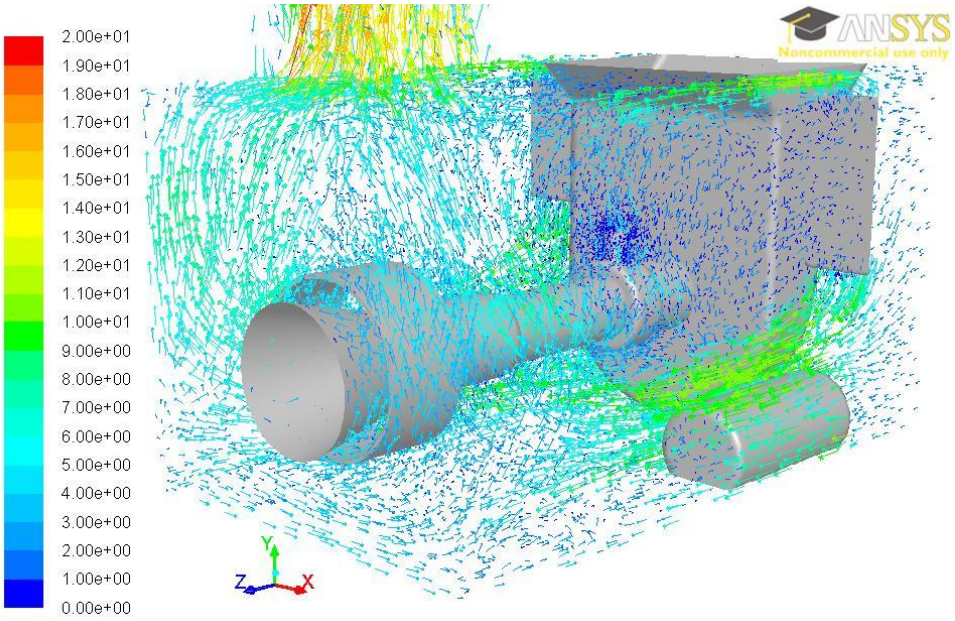

Figure 5.9 – Velocity vectors coloured by velocity magnitude (m/s) for the model without boost compressor air bleed, t = 5s

Figure 5.10 shows the velocity vectors for the model with boost compressor air bleed. The boost compressor air is bled into the overall package ventilation at a very high velocity (~200m/s). The vectors show that the jet of bleed air hits the ceiling of the package and is dispersed radially outwards along the ceiling. Some of the bleed air travels back towards the inlet where it meets the air flowing from the inlet, and is then forced under the side panels and back into the package. Only a small percentage of the boost compressor air takes the most direct path to the outlet. Most of the air is forced into the main body of the package where it interacts with the ventilation air. The scale on this picture is 0 to 220m/s and the average velocity inside the package is 9.7 m/s.

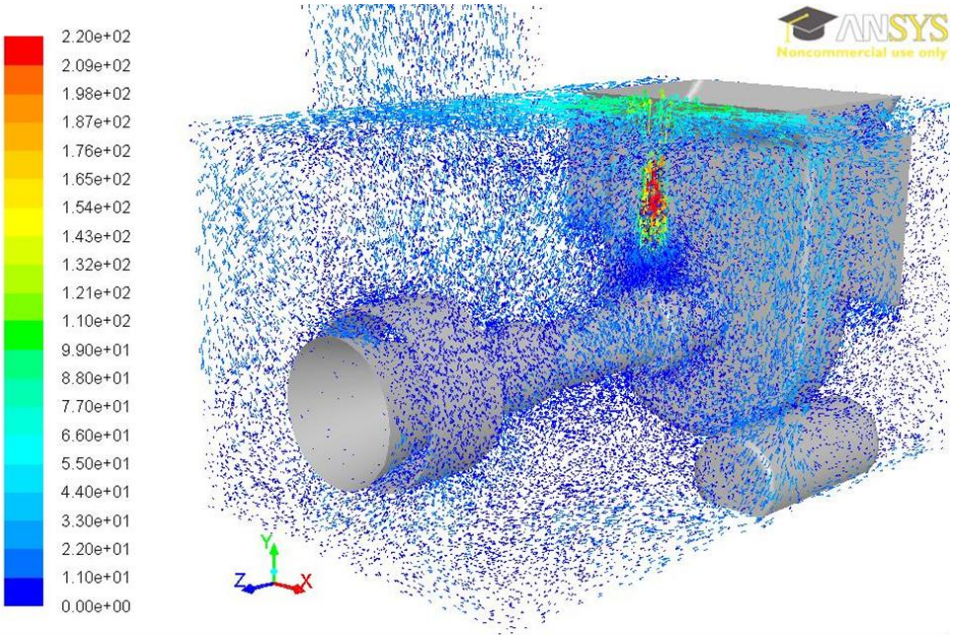

Figure 5.10 – Velocity vectors coloured by velocity magnitude (m/s) for the model with boost compressor air bleed, t = 5s

5.3.1 Analysis

As the two models do not have the same scales, care should be taken when directly comparing Figure 5.10 and Figure 5.9. Nevertheless, some general comments about the flow inside the package can be made. Firstly, the flow in the model without boost compressor air bleed is relatively orderly whereas with the addition of boost compressor air, the flow inside the package becomes more chaotic and the air inside the package experiences a higher level of mixing. Secondly, with the addition of boost compressor air bleed, the average air velocity inside the package more than doubles; increasing from 4.1 m/s to 9.7 m/s.

5.4 Velocity

The bottom face of the model has been modeled with a symmetry boundary condition, as this face is where the tread plate is located on the CX501 package. Underneath the tread plate is a dense network of pipes and so consequently the air flowing on this face will be responsible for the dispersion of any minor gas leaks from these pipes. Figure 5.11 shows the velocity contours on the bottom face of both models. The model without boost compressor air bleed is the image on the left and the model with boost compressor air bleed is on the right – the scale for these models is from 0 m/s to 22 m/s. Without boost compressor air bleed, the highest velocity on this face is where the air is forced under the combustion air inlet. On the model with boost compressor air bleed there are two areas of high velocity magnitude either side of the turbine. These areas are where the boost compressor air bleed has been dispersed along the ceiling, flows down the walls either side of the package, and then impacts with this face.

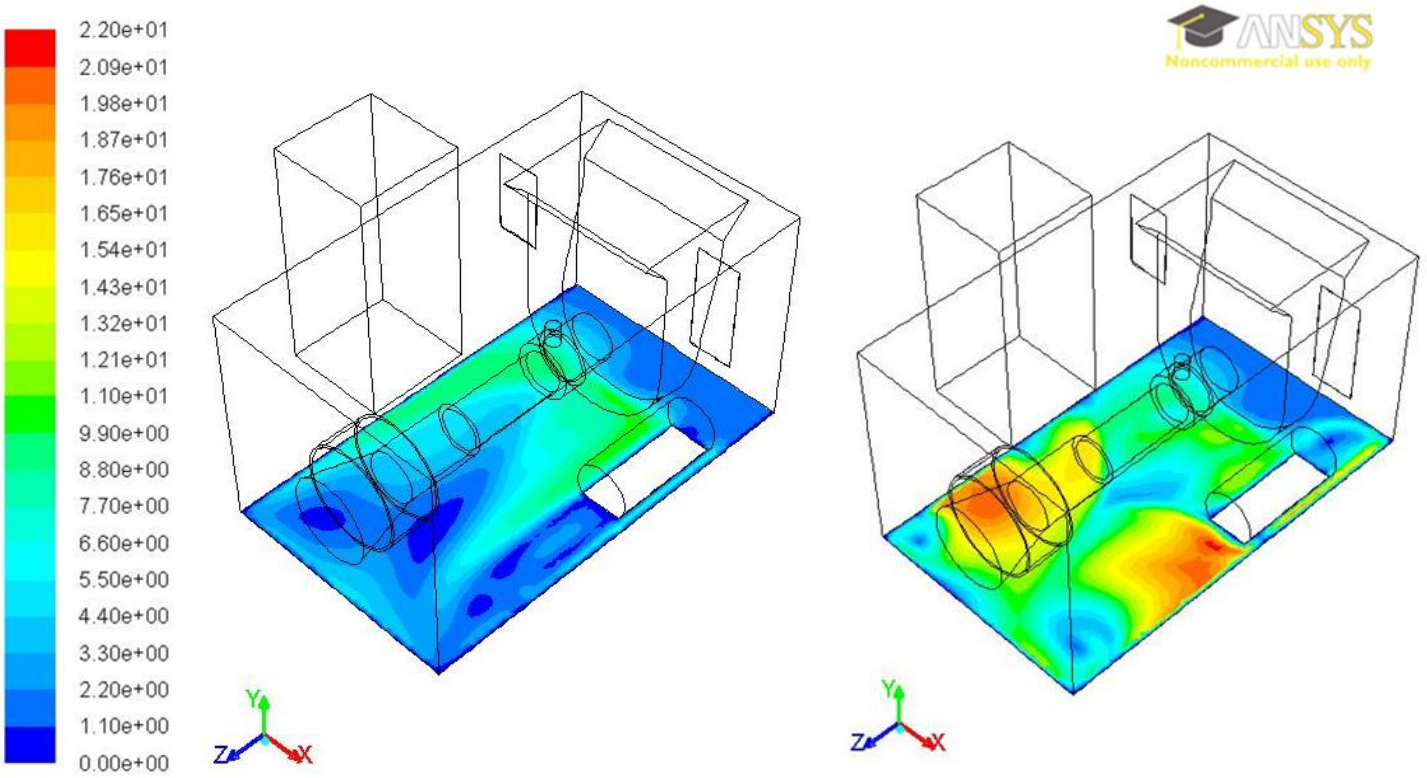

Figure 5.11 – Contours of velocity magnitude (m/s) on the bottom face for both models, without boost compressor air bleed (left) and with boost compressor air bleed (right), t = 5s

5.4.1 Analysis

In Figure 5.11 both models have the same velocity scale so the pictures are directly comparable. From this figure it is evident that the flow speed on this face has increased with the addition of boost compressor air bleed; the average flow speed on this face increases from 4.4 m/s to 9.7 m/s - this is not the result that was expected. The fan is a fixed volumetric flow rate fan, thus adding the boost compressor air bleed into the overall package ventilation reduces the air drawn through the package by the ventilation fan. Consequently it was expected that the velocity across the bottom face would decrease with the addition of boost compressor air bleed. Conversely, the boost compressor air bleed is emitted at such a high velocity that it hits the ceiling, is forced down, and mixes with the ventilation air on the bottom face of the package. As a general rule, 1m/s is the minimum airspeed required to sufficiently disperse gas leaks. An average velocity of 9.7 m/s, for the model with boost compressor air bleed, this is more than sufficient to disperse gas leaks. However, an increased flow speed on this face could potentially mask a more serious gas leak, which might prevent the leak being detected.

5.5 Package Temperature

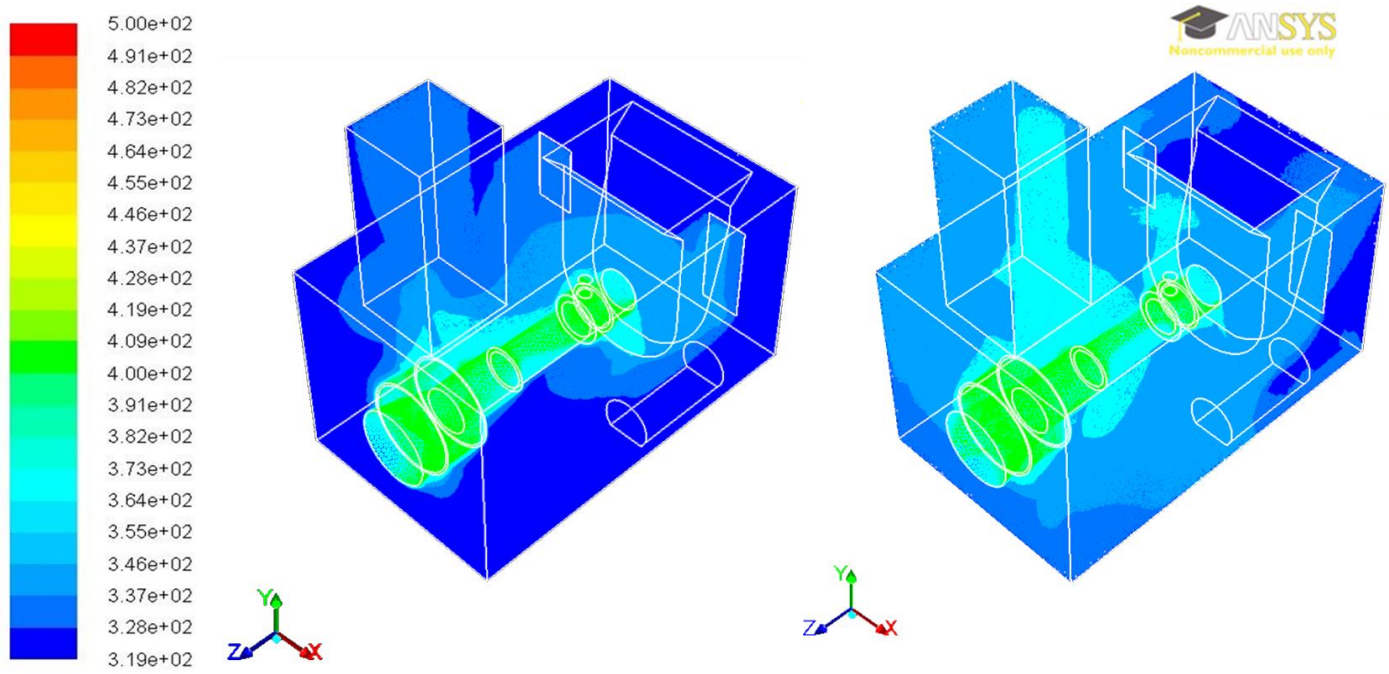

Figure 5.12 – Contours of total temperature (K) for both models, without boost compressor air bleed (left) and with boost compressor air bleed (right), t = 5s

The contours of total temperature for both models can be seen in Figure 5.12. The model without boost compressor air bleed is shown on the left, and the model with boost compressor air bleed is positioned on the right - the scale for these models is from 319K to 500K. For the model with boost compressor air bleed the average outlet temperature is 328.8K, which means the package ventilation air temperature has increased by 10.8K. The average temperature at the outlet of the model without boost compressor air bleed is 343.7K; which is a temperature increase of 24.7K.

5.5.1 Analysis

The contours of total temperature in the whole package can be seen by comparing the images in Figure 5.12. This figure shows that the temperature inside the package increases with the addition of boost compressor air bleed. The boost compressor air bleed results in an outlet temperature that is 15K higher than the model without boost compressor air bleed. The increase in overall package temperature has two main causes. Firstly the boost compressor air bleed is at a temperature of 348K which heats the overall package air. Secondly as the package is ventilated by a fixed volumetric flow rate fan, adding the boost compressor air bleed reduces the overall bleed air mass flow rate from 11 kg/s to 7.3kg/s. This is a 34% reduction in ventilation air to remove rejected heat from the gas turbine engine. The allowable temperature at the outlet of the model is governed by the operating requirements of the ventilation fan. The ventilation fan has a maximum permissible temperature of 70°C (343K). The model without boost compressor air bleed is operating at this maximum temperature, but

when boost compressor air bleed is added the outlet temperature exceeds the maximum allowed. If the fan were to be used outside of its operating requirements a volumetric flow rate of 9.7 m^3/s would not be guaranteed.

5.6 Temperature around the Turbine

One of the key roles of the package ventilation is to ensure the air surrounding the engine is at an acceptable temperature. Rolls-Royce state that the maximum surrounding air temperature (at a distance of 50mm away from the engine casing) is 344K for the compressor and boost compressor, and 477K for the combustion chamber and turbine section. Figure 5.13 shows the temperature contours around the gas turbine engine for both models; without boost compressor bleed air is shown on the left and with boost compressor bleed air is located on the right. The plane shown is the y-z plane which bisects the model. Without boost compressor bleed air the maximum surrounding air temperature around the compressor and boost compressor is approximately 380K - with bleed air this value is 360K. Without boost compressor bleed air the maximum surrounding air around the turbine and combustion chamber casing is approximately 430K - with boost compressor bleed air this value is 410K.

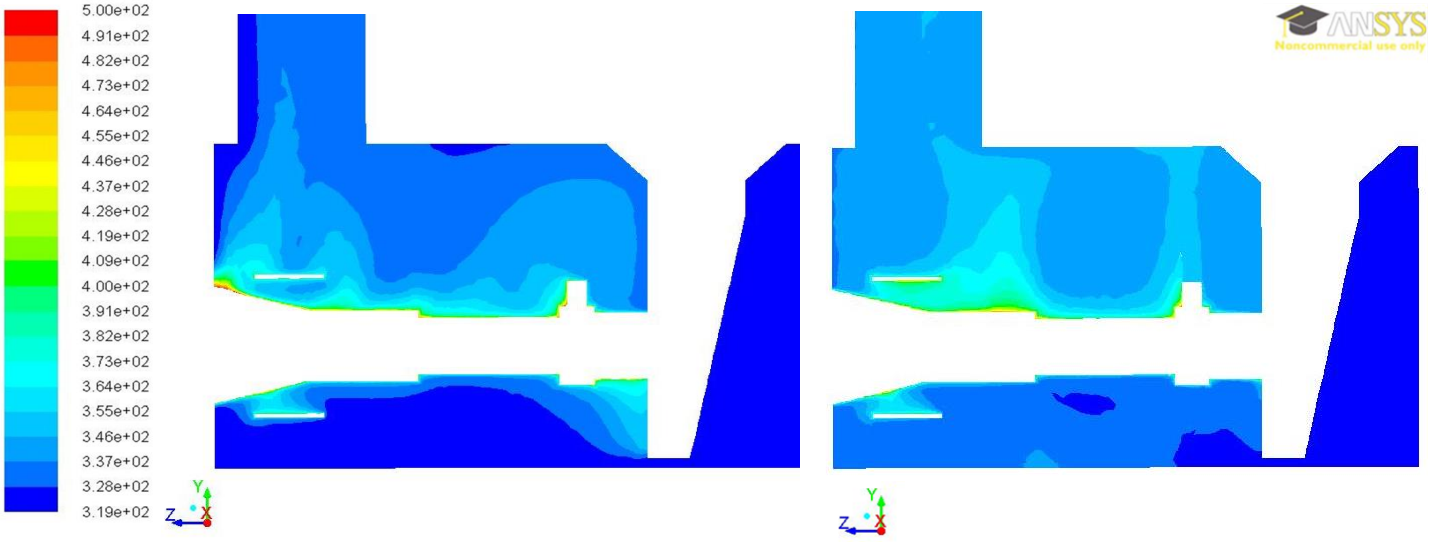

Figure 5.13 – Contours of total temperature (K) on the y-z plane which bisects the model, without boost compressor air bleed (left) and with boost compressor air bleed (right), t = 5s

5.6.1 Analysis

Comparing the two images in Figure 5.13 gives an indication of how adding boost compressor bleed air affects the airflow and heat transfer around the gas turbine engine. It is evident that with the addition of boost compressor air bleed, the average temperature of the surrounding air increases. Nevertheless, there is a decrease in the maximum temperature of the surrounding air. This is because adding boost compressor air bleed increases the mixing of the ventilation air, which helps to disperse stagnant points in the ventilation flow. Figure 5.13 reveals that the model without boost compressor air bleed has a high air temperature where the top of the turbine meets the package wall and also where the bottom of the boost compressor meets the

combustion air inlet. However these pockets of high temperature air, where there is a low flow rate, are absent from the model with boost compressor air bleed.

Both models meet the operating requirements set by Rolls-Royce for the maximum air temperature surrounding the turbine and combustion chamber. However the maximum air temperature surrounding the compressor and boost compressor is too high for both models. This is most likely due to the discrepancies between the CFD model and the actual package. The model that was compared with experimental results had a lower outlet temperature than test results. This suggests that the ventilation air in the CFD model does not remove as much heat from the engine as the ventilation air in the actual package. This is one possible explanation why the maximum air temperature surrounding the compressor and boost compressor is greater than the permissible maximum, for the model without boost compressor air bleed. Regardless of this, adding boost compressor air bleed to the overall package ventilation actually appears to lower the maximum surrounding temperature rather than increase it.

5.7 Errors and Uncertainties

5.7.1 Physical Approximation Errors

Physical approximation errors are caused by discrepancies between the CFD model and the actual model (CFD models are always an estimate of the real model). In this project not every single pipe, flange, and bolt has been resolved in the model mesh as this would be too computationally expensive. Instead, the models produced in this report are an approximation of the final model. Choosing the best approximations to represent the model is one of the challenges of CFD modeling.

5.7.2 Model Uncertainty

There are uncertainties associated with the modeling used by the CFD software. One example of this is turbulence modeling. Indeed, there are numerous turbulence models available in FLUENT because it is a difficult quantity to model. Care has been taken to reduce the uncertainty in the models used in this project by comparing the various: turbulence models, buoyancy models, and solvers; with experimental results to see which models give the most accurate results.

5.7.3 Discretisation Errors

Discretiation errors in CFD are those that occur from discretising the governing Navier-Stokes equations. These errors are the difference between the exact solutions of the partial differential equations governing fluid flow, and the exact solutions of the equations used to approximate fluid flow over a finite number of control volumes. Consequently, as the mesh gets finer (i.e. the control volumes decrease in size) the size of the discretisation errors reduces. To reduce these errors numerous mesh refinement studies have been performed throughout this project to

determine the most suitable mesh size, and the quality of the elements in the mesh have been checked and deemed satisfactory.

5.7.4 User Errors

Sources of user error include, for example, inputting incorrect inputs and boundary conditions in the case set-up, such as applying a turbulence model to a flow which is laminar. Care has been taken to reduce the user error in this project by paying attention to the User Guide and Theory Guide provided by ANSYS. The CFD models created in this project have also been compared with theoretical results, which has helped to ensure appropriate conditions were chosen for the final model.

6 Sustainability

Figure 6.1 is a graph of output power and efficiency plotted against the combustion air inlet temperature for the Rolls-Royce KB7S gas turbine engine (used in the CX501 package). This graph indicates that as the temperature of the combustion air (at the inlet to the gas turbine) increases the power output and the efficiency of the gas turbine engine decreases. The power output of the gas turbine engine depends on the mass flow rate of the air flowing through it. As the compressor operates at a constant volumetric flow rate, it is the density of the air that dictates the mass flow rate through the gas turbine engine. As the temperature of the air increases, the density of the air decreases and therefore the mass flow rate of the air also decreases. It is the mass of air which drives the gas turbine blades and so a reduction in mass flow rate of the combustion air results a reduction in power output and efficiency of the gas turbine engine. Moreover, more energy is required to compress the combustion air at higher temperatures.

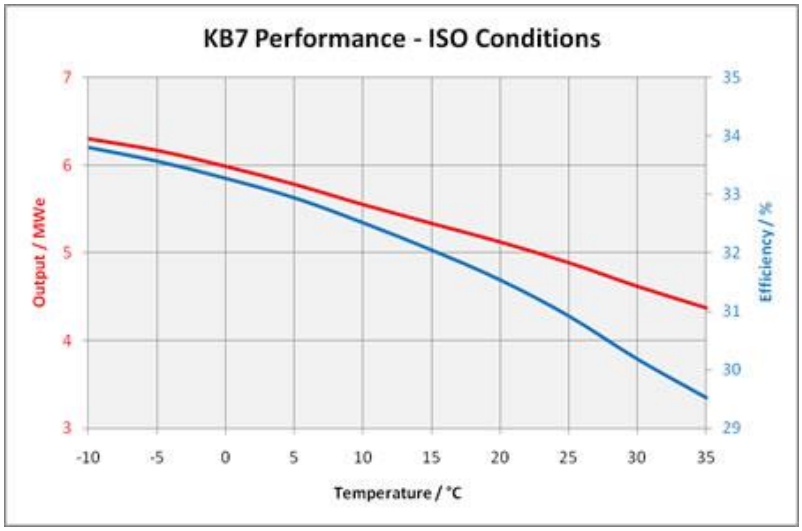

Figure 6.1 – Performance graph for KB7S gas turbine engine [33]

Centrax want to bleed air from the boost compressor (in addition to bleeding air from the 14th stage of the compressor) in order to operate the gas turbine engine at up to 50% part load. Running the gas turbine engine at part load reduces the emissions from the gas turbine engine as it is operating at less than full power. In future this project could be extended to assess whether more than 20% of the air could be bled from the boost compressor. Bleeding a higher proportion of air from the boost compressor rather than the 14th stage of the compressor, would improve the energy efficiency of the gas turbine when operating at part load. When air is bled from the 14th stage of the compressor it is fed directly into the combustion air intake. After compression, this bleed air is at a higher temperature than the ambient air so the bleed air increases the temperature of the combustion air, thereby reducing the efficiency of the gas turbine engine. The significant advantage of bleeding air from the boost compressor is that it is bled straight into the package ventilation and therefore it does not affect the combustion air inlet temperature. Additionally, when air is bled from the 14th stage of the compressor it has been compressed in the boost compressor and the compressor. The energy required to compress the bleed air is therefore wasted. Thus the second advantage to bleeding air from the boost compressor is that the air has only been compressed in the boost compressor, consequently it wastes less energy. Thus bleeding a higher proportion of air from the boost compressor would improve the energy efficiency of the gas turbine engine, and reduce the carbon emissions from the CX501 package when operating at part load.

7 Conclusions

In conclusion, this project has successfully used CFD to model the ventilation air in the CX501 package. Two CFD models of the package ventilation, with and without boost compressor air bleed, were compared. This comparison enabled several comments to be made on the feasibility of adding boost compressor air bleed into the package ventilation. Firstly the outlet temperature of the ventilation air, for the model with boost compressor air bleed, was 343.7K; this is 15K higher than the model without boost compressor air bleed. The outlet temperature of the ventilation air is above the operating range for the ventilation fan used in the CX501 package. Therefore in order to bleed air from the boost compressor Centrax would need to source a ventilation fan that could operate at higher temperatures.

Secondly adding boost compressor air bleed to the package ventilation increased the average velocity on the surface of the tread plate from 4.4 m/s to 9.7 m/s. An average velocity of 9.7 m/s is more than sufficient to disperse any minor gas leaks. However, an increase in air velocity on the tread plate could potentially mask a more serious gas leak, which might prevent the leak being detected. Centrax would need to investigate the safety implications of this increase in velocity on the tread plate, before adding boost compressor air bleed into the package ventilation.

Thirdly adding boost compressor air bleed caused greater mixing of the ventilation air within the package, which prevented hot pockets of air forming in areas of low velocity air around the gas turbine engine. As a result of this increased mixing, the maximum air temperature surrounding the gas turbine engine decreased despite an increase in the average air temperature surrounding the gas turbine engine. On both CFD models the maximum air temperature surrounding the compressor and boost compressor was higher than the permitted maximum. One possible reason for this is the physical discrepancies between the CFD models and the actual CX501 package. Further work on the CFD models would be necessary to improve the physical accuracy of the CFD models.

When the final model was compared with test data provided by Centrax, it was found that the outlet temperature of the ventilation air was 3.6K lower than the test results. The lower ventilation air outlet temperature suggests that the heat transfer from the gas turbine engine to the package ventilation air is less than it should be in the CFD models. This is most probably due to physical errors rather than computational errors. In future, it would be necessary to investigate different techniques to model the surface of the gas turbine engine. It would be too computationally expensive to model every object that covered the surface of the gas turbine engine. However one possible way would be to create a semi-porous region around the gas turbine engine, which would mimic the effect of the surface of the engine on the ventilation air flow. It would also be essential to carry out more validation studies on the CFD models, to corroborate the results provided by CFD with test data from Centrax.

8 References

[1] *Centrax Gas Turbines | Publications*. [online] Available at: http://www.centraxgt.com/images/stories/273_Brochure_General.pdf [Accessed 01/08/2012].

[2] *Rolls-Royce | Energy Product Gas Turbines* | 501. [online] Available at: http://www.rolls-royce.com/energy/energy_products/gas_turbines/501/ [Accessed 02/02/2013].

[3] Centrax Gas Turbines. *CFD Analysis of CX501 Generator Set Package Ventilation Initial Project Meeting.* 10th October 2012.

[4] ANSYS, Inc., ANSYS FLUENT (Version 14.5) [Computer program].

[5] Versteeg, H.K., and Malalalsekera, W., 2006. *An introduction to computational fluid dynamics: the finite volume method*. 2nd ed. Harlow: Prentice Hall.

[6] Versteeg, H.K., and Malalalsekera, W., 2006. *An introduction to computational fluid dynamics: the finite volume method.* 2nd ed. Harlow: Prentice Hall. Chapter 1.

[7] Sun, Z. and Wang, S., 2010. *A CFD-based test method for control of indoor environment and space ventilation.* Building and Environment, **45**(6): p. 1441-1447.

[8] Launder, B.E., and Spalding, D.B., 1974. *The numerical computation of turbulent flows. Computer Methods in Applied Mechanics and Engineering,* **3**(2): p. 269-289.

[9] Ivings, M.J., Lea, C.J., and Ledin, H.S., 2003. *Outstanding safety questions concerning the analysis of ventilation and gas dispersion in gas turbine enclosures: Best Practise Guidelines for CFD.* [pdf] Available at: http://www.hse.gov.uk/research/hsl_pdf/2003/cm03-12.pdf [Accessed 11/11/2012].

[10] Behnia, M., Nakayama, W., et al., 1998. *CFD simulations of heat transfer from a heated module in an air stream: Comparison with experiments and a parametric study.* In: IEEE (Institute of Electrical and Electronic Engineers), Proceedings of the 1998 6th Intersociety Conference on Thermal and Thermomechanical Phenomena in Electronic Systems: p. 143-151. Seattle, 27th – 30th May 1998. IEEE.

[11] Li, Q., et al., 2009. *CFD study of the thermal environment in an air-conditioned train station building.* Building and Environment, **44**(7): p. 1452-1465.

[12] Stamou, A., and Katsiris, I., 2006. *Verification of a CFD model for indoor airflow and heat transfer.* Building and Environment, **41**(9): p. 1171-1181.

[13] Defraeye, T., B. Blocken, et al., 2010. *CFD analysis of convective heat transfer at the surfaces of a cube immersed in a turbulent boundary layer.* International Journal of Heat and Mass Transfer, **53**(1–3): p. 297-308.

[14] Vahidi, D., Bagheri, H., et al., 2006. *Numerical and experimental study of ventilation for turbine package enclosure.* Proceedings of the ASME Turbo Expo, 5(A): p.607-616.

[15] Santon, R.C., et al., 2000. *Studies into the role of ventilation and the consequences of leaks in gas turbine power plant acoustic enclosures and turbine halls.* Process Safety and Environmental Protection, **78**(B3): p. 175-183.

[16] Casey, M. and Wintergerste, T. (Eds.), 2000. *Best Practices Guidelines (Version 1.0),* ERCOFTAC (European Research Community on Flow, Turbulence and Combustion) Special Interest Group on Quality and Trust in Industrial CFD.

[17] Incropera, F.P., and DeWitt, D.P., 1996. *Fundamentals of Heat and Mass Transfer*. 4th ed. New York: John Wiley & Sons. Chapter 1.

[18] ANSYS, Inc., 2012. *ANSYS FLUENT Theory Guide 14.5* [pdf] Available through: ANSYS Customer Portal <https://support.ansys.com/portal/site/AnsysCustomerPortal> [Accessed 11/02/2013] Section 4.13 *Near-Wall Treatments for Wall-Bounded Turbulent Flows.*

[19] ANSYS, Inc., 2012. *ANSYS FLUENT User Guide 14.5* [pdf] Available through: ANSYS Customer Portal <https://support.ansys.com/portal/site/AnsysCustomerPortal> [Accessed 11/02/2013] Section 12.2 *Choosing a Turbulence Model.*

[20] Tabor, G., 2012. *Fluid Mechanics Lecture 6,* Thermofluids and Energy Conversion, ECM3110/3111. [online via internal ELE] The University of Exeter. Available at: http://vle.exeter.ac.uk/file.php/747/ECM31101/fluidsStudyResources/slides/lecture6-slides.pdf [Accessed 15/01/2013].

[21] Mishra, A.K., Nawal, S., and Thundil Karuppa Raj, R., 2012. *Heat Transfer Augmentation of Air Cooled Internal Combustion Engine Using Fins Through Numerical Techniques.* Research Journal of Engineering Sciences, **1**(2): p. 32-40.

[22] Incropera, F.P., and DeWitt, D.P., 1996. *Fundamentals of Heat and Mass Transfer.* 4th ed. New York: John Wiley & Sons. Chapters 6 & 7.

[23] University of Exeter, 2013, *DSE Workstation Self-Assessment,* [online] Available at: http://www.exeter.ac.uk/staff/wellbeing/safety/formssignsandtemplates/[Accessed 20/01/2013].

[24] Zeytounian, R. K., 2003. *Joseph Boussinesq and his approximation: a contemporary view.* Comptes Rendus Mécanique, **331**(8): 575-586.

[25] Lee, Y., and Kim, K. C., 1993. *An analysis of transverse convex curvature on turbulent flow and heat transfer.* Wärme und Stroffübertagung (Heat and Mass Transfer), **28**(1-2): p. 89-95.

[26] CFD Online, 2012. *Courant-Friedrichs-Lewy condition.* [online] Available at: http://www.cfd-online.com/Wiki/Courant%E2%80%93Friedrichs%E2%80%93Lewy _condition [Accessed 02/02/2013].

[27] ANSYS, Inc., 2012. *ANSYS FLUENT User Guide 14.5* [pdf] Available through: ANSYS Customer Portal <https://support.ansys.com/portal/site/AnsysCustomerPortal> [Accessed 11/02/2013] Section 28.3 *Pressure Based Solver Settings.*

[28] Barton, I. E., 1998. *Comparison of SIMPLE- and PISO-type algorithms for transient flows.* International Journal for Numerical Methods in Fluids **26**:459 - 483.

[29] ANSYS, Inc., 2012. *ANSYS FLUENT User Guide 14.5* [pdf] Available through: ANSYS Customer Portal <https://support.ansys.com/portal/site/AnsysCustomerPortal> [Accessed 11/02/2013] Section 5.2 *Mesh Requirements and Considerations.*

[30] Ghiaasiaan, M., 2011. *Convective Heat and Mass Transfer*. New York: Cambridge University Press. Chapter 7.

[31] ANSYS, Inc., 2012. *ANSYS FLUENT User Guide 14.5* [pdf] Available through: ANSYS Customer Portal <https://support.ansys.com/portal/site/AnsysCustomerPortal> [Accessed 11/02/2013] Section 6.3 *Boundary Conditions.*

[32] Walker, P., Pete.Walker@centraxgt.com, 2013, *CX501 Ventilation Project*. [email] Message to Heather Bolt (hk282@exeter.ac.uk) Sent 22/03/2013, 13:52.

[33] *Centrax Gas Turbines | Products | Generator Set Type CX501- KB7*. [online] Available at: http://www.centraxgt.com/index.php/products/cx501-kb7?lang=en [Accessed 02/02/2013[

[34] University of Exeter, 2013, *Risk Assessment Form,* [online] Available at: http://www.exeter.ac.uk/staff/wellbeing/safety/formssignsandtemplates/[Accessed 20/01/2013].

[35] Bolt, H., 2012. *Preliminary Report: CFD Analysis of CX501 Generator Set Package Ventilation for Centrax Gas Turbines.*

9 Appendices

9.1 Appendix A – Nusselt Number Correlation Studies

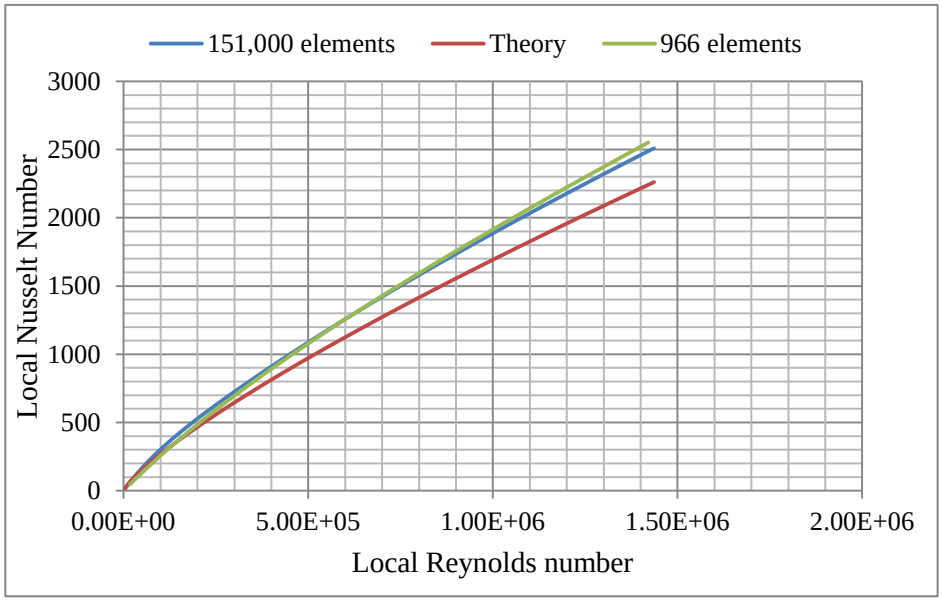

Figure A.1 – Graph of local Nusselt number plotted against local Reynolds number for Model 1.

Figure A.1 reveals that increasing the number of elements in the global mesh from 966 to 151,000 has little effect on the accuracy of the local Nusselt number for Model 1.

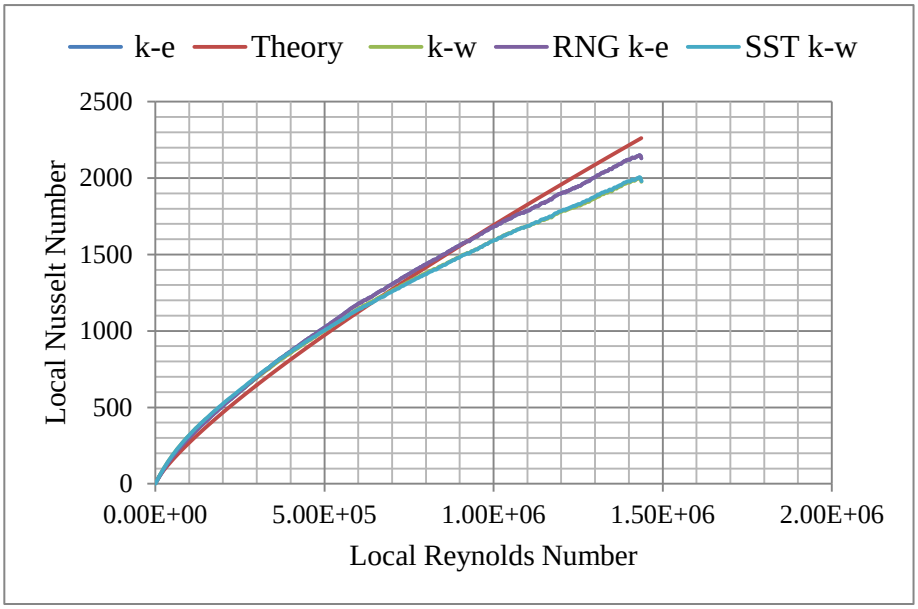

Figure A.2 - Graph of local Nusselt number plotted against local Reynolds number, for Model 1, showing different turbulence models.

Different turbulence models were tried for Model 1. Figure A.2 reveals that there is no difference between the k-ε and the RNG k-ε models, there is also no difference between the k-ω and SST k-ω models. The k-ε models show best agreement with theory.

9.2 Appendix B – Surface Temperatures

Table B.1- Surface temperatures of gas turbine engine and scatter shield

Surface	Temperature (K)
Boost Compressor	644
Compressor	644
Combustion Chamber	709
Turbine	823
Scatter Shield Inner Surface	623
Scatter Shield Outer Surface	523
Scatter Shield Sides	573

9.3 Appendix C – Graph of Residuals

The residuals for the final model without boost compressor air bleed have been plotted in 3 graphs, as these are the graphs provided by FLUENT. The graph of residuals for the model with boost compressor air bleed was very similar, and therefore has not been included in this appendix. The residuals appear to be spaced closer together towards the end of the graph, this is because of the way the auto save function works in FLUENT. FLUENT only saves a maximum of 1,000 iterations by default (to save space), when this target is reached it deletes every other iteration and plots a further 500 iterations, thus residual data is lost at the beginning of the calculation.

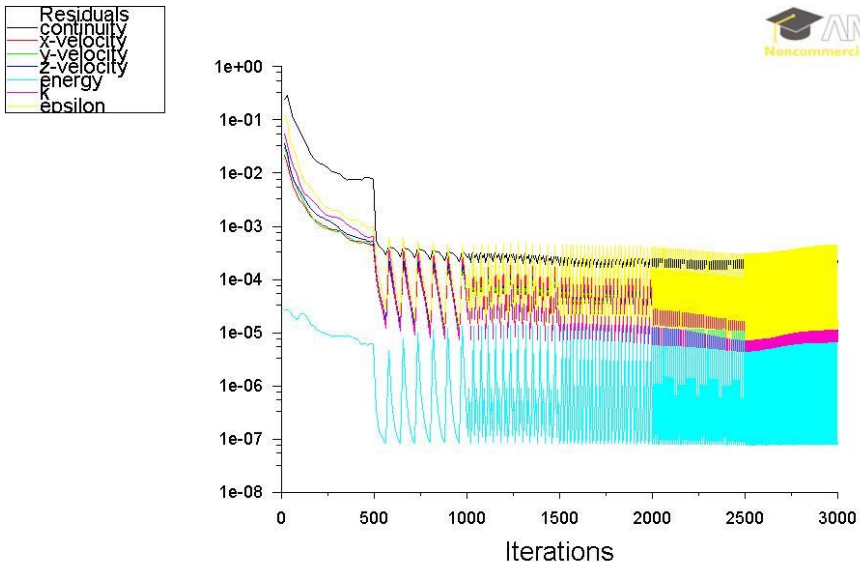

Figure C.1 – Graph of residuals for the final model without boost compressor air bleed; 0-3,000 iterations (0-1s)

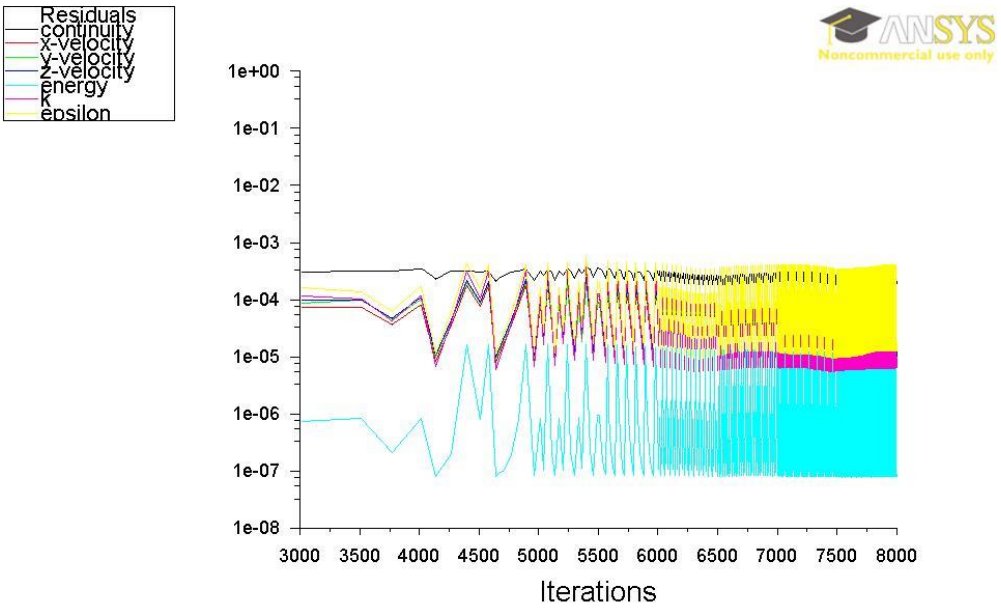

Figure C.2 - Graph of residuals for the final model without boost compressor air bleed; 3,000 to 8,000 iterations (1-3s)

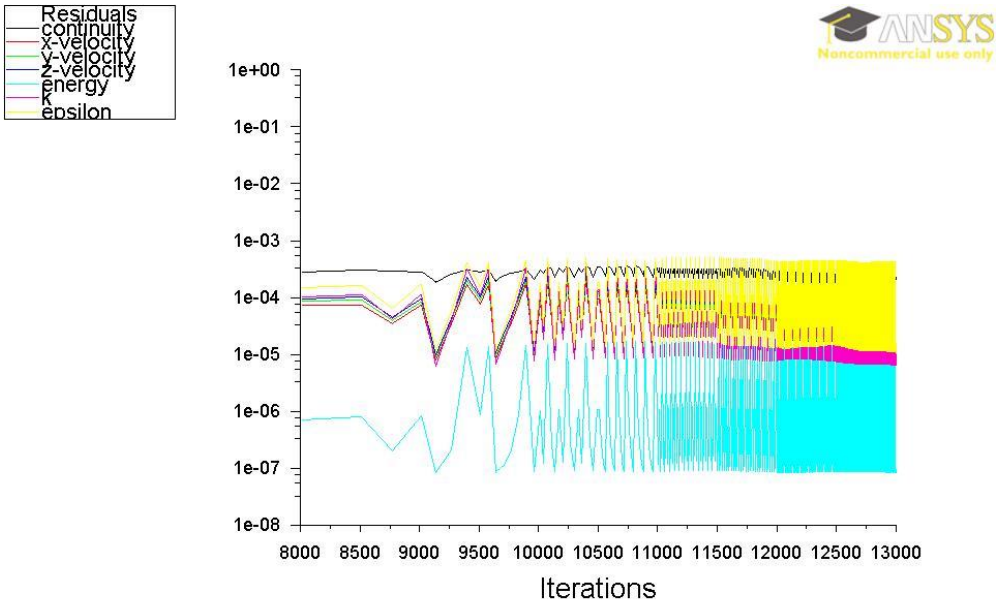

Figure C.3 - Graph of residuals for the final model without boost compressor air bleed; 8,000 to 13,000 iterations (3-5s)

9.4 Appendix D – Health and Safety Risk Assessment

(Template by the University of Exeter [34])

THE MANAGEMENT OF HEALTH AND SAFETY AT WORK REGULATIONS (1992) HAZARD IDENTIFICATION / RISK ASSESSMENT FORM

SECTION ONE ADMINISTRATIVE DETAILS

REFERENCE: Heather Bolt Individual Project	
DEPARTMENT: CEMPS	**SIGNATURE OF HEAD OF DEPT:** N/A
DATE: 10/10/12	**ASSESSED UNDER OTHER REGULATIONS?** YES ☐ NO ☒
REMEDIAL ACTION REQUIRED? YES ☐ NO ☒	**OTHER ASSESSMENT REFERENCE:** N/A
REMEDIAL ACTION PRIORITY? **HIGH** ☐ **MEDIUM** ☐ **LOW** ☐	

WORK ACTIVITY:
Working in Harrison: 207/ 208/ RED Room.

BRIEF DESCRIPTION:
This project involves using ANSYS FLUENT, CFD software only available on the computers in Harrison: 207, 208 and the RED Room. This will involve long periods of time using the computers in these rooms.

This is an office based Risk Assessment form – there is no use of the workshops involved in this project.

SECTION TWO HAZARD IDENTIFICATION

HAZARD = something with the potential to cause harm

- **Identify HAZARDS, circle KEYWORDS**

HAZARDS	KEYWORDS
Physical	
Confined Space	asphyxiant cold hot toxic irritant lone working ventilation
Building Related	CONDAM Regs Ass't scaffolding work at height falling object asbestos containing materials
Display Screen Equip't	DSE Regs Ass't desk chair electricity eye strain eye test posture
Electricity	PAT testing live static induced arc heat burn shock 240V AC 405V AC high voltage
Environment	temperature humidity light sound space
Fire	flammable combustible explosion oxygen heat
Handling	MHO Regs Ass't abrasive heavy lifting pushing pulling sharp hot cold awkward
Heat / Cold	radiation conduction convection burn scald touch
Housekeeping	falling tripping slipping storage space cables combustion sources hygiene
Machinery	MHO Regs Ass't cutting rotating sliding falling entrapment breakage ejection of parts electricity radiation heat cold
Movement	slip fall trip wet ice steps stairs height
Pressure / Vacuum	burst release lines joints container cylinder explosion leak blockage relief/control failure
Radiation (Ionising)	radioisotope X-ray alpha beta gamma contamination exposure use storage disposal
Radiation (Non Ionising)	ultra-violet infra-red laser microwave burns welding eye cataract
Transport	road markings road signs dangerous loads minibus fork-lift truck trolley truck commercial vehicle passenger lift goods lift footpath ramp car boat
Water	diving drowning slipping electricity
Weather	hot cold wet ice wind lone-working frost-bite heat-stroke sunburn skin cancer hypothermia
Chemical	
Physical state	solid dust liquid gas vapour fume hot cold
Properties	COSHH Ass't toxic corrosive irritant carcinogen allergen flammable unstable explosive
Routes of Entry	inhalation ingestion skin contact
Biological	
Type	COSHH Ass't micro-organism bacteria virus parasites cell culture storage disposal
Properties	infectious pathogenic carcinogenic mutagenic teratogenic storage disposal
Genetic modification	GMO Regs Ass't storage disposal
Psychological	
Type	fatigue stress trauma

SECTION THREE **RISK ASSESSMENT**

RISK = a combination of the likelihood a hazard will cause injury and the severity of the injury

- Quantify risk for each hazard identified using the following table.

Likelihood of injury	*Score A*	Severity of injury	*Score B*
improbable	*1*	very minor injury; abrasions / contusions	*1*
remote	*2*	minor injuries; cuts / burns	*2*
possible	*3*	major injuries; fractures / cuts / burns / damage to internal organs	*3*
probable	*4*	severe injury; amputation / eye loss / permanent disability	*4*
likely	*5*	death	*5*

- If **Risk** factor is 5 or under, the risks are under adequate control, but should be carefully monitored
- If **Risk** factor is over 5: take **Remedial Action** to improve **Existing control measures** or **abandon the task**

Hazards	Existing control measures	*Score A*	*Score B*	Risk (A x B)	Remedial Action
Display Screen Equipment Working intensely at a computer can cause pain from repetitive strain injury or bad posture.	• Take regular breaks to move around and stretch legs and prevent RSI. • Read through DSE advice supplied by the University of Exeter Available at: http://www.exeter.ac.uk/staff/wellbeing/safety/formssignsandtemplates/. • Position monitor, keyboard and mouse in order to ensure good posture. • Wear glasses (if necessary).	4	1	4	NONE
Fire If trapped in Harrison Building upon a fire there is risk of injury.	• Be familiar with the University's Fire Evacuation Policy, make note of Fire Exits and Fire Alarm Points.	1	2	2	NONE
Lone Working Possibility of injury or falling ill while working alone.	• Don't work in Harrison alone (as dictated in University Policy).	1	2	2	NONE
Stress	• Take sufficient breaks while working. • Avoid over-working/ working excessive hours.	3	1	3	NONE
Electrical Electrical shock from faulty equipment.	• All University equipment is PAT tested. • Report faulty plugs sockets/ electrical equipment to Department of Infrastructure and Technical Services.	1	3	3	NONE
Environment Poor lighting/ ventilation can cause discomfort and headaches	• Ensure suitable room conditions by adjusting air con/ lighting/ window blinds.	2	1	2	NONE

9.5 Appendix E – Project Risk Assessment [35]

ID	Risk item	Effect	Cause	Likelihood	Severity	Importance	Action to minimise risk
	Describe the risk briefly	*What is the effect on any or all of the project deliverables if the cause actually happens?*	*What are the possible cause(s) of this risk?*	*/10*	*/10*	*L*S*	*What action(s) will you take (and by when) to prevent, reduce the impact of, or transfer the risk of this occurring?*
1	Model will not mesh properly.	This could cause one or more of the critical tasks to overrun affecting the overall project end time.	1. Geometry has been imported from Solidworks. 2. Poor geometry.	7	5	35	1. Create all geometry using Design Modeller app in Fluent. 2. Refine mesh around more complicated aspects of geometry.
2	Solution will not converge.	This could cause one or more of the critical tasks to overrun affecting the overall project end time.	Poor mesh, errors with set-up e.g. boundary conditions	8	6	48	Start with an oversimplified model and increase complexity gradually.
3	Centrax take longer than expected to provide essential information (e.g. temperature of turbine casing).	This could delay the completion of one or both of the models.	Centrax waiting on information from third party such as Rolls-Royce.	7	4	28	Estimate missing values and then amend model when information is provided to prevent project overrunning,
4	Centrax take longer than expected to provide test results.	Model 1 would not be verified by Centrax test data. This may or may not cause issues later on in the project.	CX501 test is postponed or has to be repeated due to errors.	6	5	30	If the test data is not available when model 1 is completed the project will have to continue and model 1 will need to be verified at a later date. If computational and experimental results concur then no action will be taken, if not then model 1 will need to be improved.
5	CFD results do not correspond to actual results.	This could delay the project significantly depending on how long it takes achieve an accurate model.	Errors in model.	6	9	54	Task 29 ‘project contingency’ has been scheduled in to compensate for delays in the project.

9.6 Appendix F – Preliminary Report